HIGH SPECTRAL RESOLUTION OBSERVATIONS OF THE MOLECULAR HYDROGEN EMISSION IN THE ORION MOLECULAR CLOUD

Thesis by

Daniel Nadeau

In Partial Fulfillment of the Requirements

for the Degree of

Doctor of Philosophy

California Institute of Technology

Pasadena, California

1981

(Submitted on December 31, 1980)

ACKNOWLEDGEMENTS

This thesis is the fruit of five years of work done in collaboration or with the help of many people whom it is a great pleasure to thank.

My adviser, Gerry Neugebauer, has taught me much about science through his strong leadership and his dedication to all the facets of scientific research. His concern for my work and his encouragements were deeply felt, and I am especially thankful for all the time he has spent reading and commenting on the many versions of this thesis. I am also grateful to him and to his wife Marcia for their warm hospitality.

Tom Geballe has participated in all the phases of this research and he has also spent much time commenting on the thesis. I am greatly indebted to him for his expertise and his patience. He and his wife Carole cheered me up on many occasions.

Tom Soifer has provided much useful criticism of this thesis. I have also enjoyed discussions with Mark Allen, Sara Beck, Eric Becklin, Steve Beckwith, Bruce Draine, Jay Elias, Ian Gatley, Reinhardt Genzel, Peter Goldreich, Dave Hollenbach, Jill Knapp, John Lacy, Keith Matthews, Guido Munch, Eric Persson, Tom Phillips, Peter Wannier, Tom Wilson, and especially Mike Werner, who has kindly given me his support throughout my graduate studies.

I have received much experimental advice and technical assistance from K. Matthews, E. Persson and Gordon Forrester. Much of the success of my observations is due to their efforts. Vagn Stephensen, Mel Kriegel and Jim Wright have done excellent work on the instrument and helped me build it in record time. This was to be one of Vagn's last projects, and I will not forget his personal

interest in my work. Dave Ennis, Kris Sellgren and Graham Berriman have assisted me at the observatory and they also gave me their friendship. The staffs of Mount Wilson, Palomar and Las Campanas Observatories, especially Juan Carrasco, Jim Frazer and Howard Lanning, have given me their enthusiastic support during my observations. As director of Mt. Wilson, George Preston has been most helpful and understanding. Judy Bennett, Barbara Zimmerman, Edith Huang and Stephen Mochnacky have provided much computer programming assistance. The help I have received from all these people had more to do with friendship than with duty, and to all of them I wish to express my gratitude.

This work has been supported by NASA grants NGL 05-002-207 and NGL 05-002-140 and by NSF grants AST77-20516 and AST78-16826. Personal financial support has been provided by graduate fellowships from the Natural Science and Engineering Research Council of Canada and by graduate research and teaching assistantships at Caltech.

Ce sont les encouragements et les marques d'affection de tous les membres de ma famille, tout au long de mes études et spécialement durant les moments les plus difficiles, qui ont, par-dessus tout, rendu possible la persévérance qui a conduit à mes succès. Je suis particulièrement reconnaissant envers mes parents, pour leur amour, pour l'éducation qu'ils m'ont donnée et pour avoir su animer et préserver un foyer stable et chaleureux, favorable au développement intellectuel. Je ne saurais suffisamment remercier enfin ma famille de Californie, qui m'a adopté de si grand coeur. Les liens qui nous unissent survivront le temps et la distance.

ABSTRACT

Observations of line profiles of the vibrationally excited H_2 gas in the Orion molecular cloud are presented. The $v=1\rightarrow 0\ S(1)$, $v=1\rightarrow 0\ S(0)$ and $v=2\rightarrow 1\ S(1)$ lines, emitted at a wavelength near 2μm, have been observed with a spectral resolution of $20\,\mathrm{km\,s^{-1}}$. The region has been mapped extensively in the $v=1\rightarrow 0\ S(1)$ line with a spatial resolution of 10" and 5", and the line has been monitored at a few positions over a period of 15 months. The profiles of the $v=1\rightarrow 0\ S(0)$ and $v=2\rightarrow 1\ S(1)$ lines have been compared at two positions.

The mapping measurements show variations from the periphery where the profiles are narrow, symmetric and have a peak velocity equal to that of the molecular cloud, to the center of the region of emission where the profiles are wide, asymmetric and blueshifted. The line profiles do not appear to vary with time or with the energy of the upper level of the transition.

The results are interpreted by a model of a radially expanding flow of gas. From a study of H_2 excitation behind a shock front and in a magnetic precursor ahead of a shock wave, it is concluded that the high velocity emission comes from the high velocity gas in the flow, and the low velocity emission comes from gas in the molecular cloud surrounding the flow, with density inhomogeneities contributing to the detailed profiles. Finally the H_2 emission is compared to the CO and H_2O maser emission and to the infrared continuum sources.

An instrument which incorporates a piezoelectrically scanned Fabry-Pérot interferometer, an InSb detector cooled to $\sim 55\,\mathrm{K}$, a rotary chopper, and an offset guider has been built to make these observations. Its operation is described in an appendix.

TABLE OF CONTENTS

INTRODUCTION

The subject of this thesis is the study of a molecule, H_2, in a relatively small part of a molecular cloud, the region of the cluster of infrared sources in the Orion molecular cloud. Molecular clouds, which may account for 50% of the mass of the interstellar medium, often have masses of the order of $10^4 M_\odot$ and probably have a propensity to collapse and to lead to star formation (Evans 1980). The interaction between a molecular cloud and the continuum sources embedded into it has become one of the most important problems of the study of the interstellar medium. The molecular cloud is probably at the origin of the formation of the continuum sources while these sources, in turn, often have a profound effect on the molecular cloud, to the point that they may disrupt it and appear as regions of ionized gas at its surface. Molecular clouds are often found by observing CO near regions of visible nebulae. The high densities characteristic of molecular clouds mean that chemical reactions and magnetic field may play important roles within the cloud.

The Orion molecular cloud is prototypical of regions of star formation, and the relationship between the sources and the cloud can be studied in detail because of the relative proximity of the cloud to earth. It contains the brightest observed source of H_2 emission. The relationship of the H_2 emission with the region of the infrared continuum sources suggests that H_2 might be a good probe of the interaction of the sources with the molecular cloud.

The importance of the H_2 molecule in astronomy comes from the fact that hydrogen dominates the abundance of all other elements, so that molecular clouds are mainly clouds of H_2, even though they are usually discovered and measured by the observation of another molecule, CO, which has an abundance relative to H_2 less than 10^{-4}. Indeed, the density of H_2 in a molecular cloud is

often derived from measurements of ^{13}CO and from an indirect knowledge of the ratio of visual extinction to the column density of H_2 gas and to the column density of ^{13}CO. This is because the H_2 molecule has a very low spontaneous transition probability, for lack of a dipole moment, and because its rotational and vibrational levels have very high energies, since H_2 is made out of the lightest element. While most other molecules have transitions at radio and microwave frequencies H_2 can only be observed in the near infrared, or in the ultraviolet through its electronic transitions. Because of the high excitation energies of H_2, this molecule is a probe of the very hot regions ($\sim$ 1000 K) of molecular clouds.

There are two main processes by which H_2 can be vibrationally excited: a transition to an excited electronic level by absorption of an ultraviolet photon, followed by a deexcitation through the vibrational levels of the ground electronic level, and collisional excitation. Beckwith (1978) concluded from measurements of the integrated intensity of the 2 μm lines of H_2 that collisional excitation by shock waves was the most likely mechanism. This implies the transformation of bulk kinetic energy into thermal energy so that motion of the gas is expected. Following the conclusion of Beckwith we have decided to study the excitation mechanism of H_2 by observing the velocity profiles of the hot gas.

This thesis presents observations of the velocity profiles of three lines of H_2 emitted near a wavelength of 2 μm. The technique employed for these observations is that of Fabry-Pérot interferometry. This technique has been used successfully in astronomy only since circa 1964, making its debut approximately at the same time as infrared astronomy. It is particularly useful for observing extended emission regions, such as nebulae and interstellar clouds, at very high spectral resolution, since the resolution of the Fabry-Pérot is not much degraded by the use of a large focal plane diaphragm. The use of stacks of

piezoelectric crystals to adjust the interferometer and to scan the spectrum, has made the Fabry-Pérot a very practical instrument. The technique of piezoelectric scanning has been developed to the point that Fabry-Pérot interferometers suitable for astronomy are now commercially available.

The results of the observations are presented in the form of two papers. Paper I, which has been published in the *Astrophysical Journal (Letters)* in collaboration with Tom Geballe, describes preliminary results showing large variations of the line profiles across the region of emission, and the presence of emission at velocities much higher than those which had been predicted and measured earlier for the excited H_2. Paper II, written in collaboration with Gerry Neugebauer and Tom Geballe, presents extensive observations of the region of emission, which are followed by a study of the motion, the distribution and the mechanisms of excitation of the molecular hydrogen observed at $2\,\mu m$.

REFERENCES

Beckwith, S. 1978, Ph.D. thesis, California Institute of Technology.

Evans, N.J. II 1980, in *Infrared Astronomy*, I.A.U. Symp. No. 96, ed. E.E. Becklin and C.G. Wynn-Williams (Dordrecht: Reidel).

PAPER I:

VELOCITY PROFILES OF THE 2.1 MICRON H_2 EMISSION LINE IN THE ORION MOLECULAR CLOUD

Published in the *Astrophysical Journal*

Volume 230, pages L169-L173

in collaboration with

T. R. Geballe

ABSTRACT

Spectra of the H_2 v = 1-0 S(1) emission line in Orion, observed at various positions with a resolution of 20 km s^{-1}, are presented. The intrinsic full width at half maximum of the line ranges from 18 to 58 km s^{-1} over the observed positions. Analysis of the line profiles shows that the emitting gas is probably expanding from a region near the BN and KL infrared sources at velocities typically of 40 km s^{-1} but as high as $\sim$ 100 km s^{-1}, and that it is associated with the sources of the broad lines seen in the spectra of many other molecules. Strong constraints are placed on models of the physical processes responsible for the broad emission lines.

SUBJECT HEADINGS: Infrared: spectra

Molecular processes

Interstellar: molecules

Nebulae: Orion Nebula

Line profiles

I. INTRODUCTION

The quadrupole emission lines of molecular hydrogen between 2.0 and 2.5 μm were detected in the Orion molecular cloud by Gautier et al. (1976). The region of emission has been mapped in the 2.12 μm v = 1-0 S(1) line by Grasdalen and Joyce (1976) and by Beckwith et al. (1978). At a resolution of 5" the S(1) line intensity is highly nonuniform and characterized by five peaks distributed more or less along a crescent of approximately one arcminute extent. It has also been shown by Beckwith et al. (1979) that the emission comes from deep within the molecular cloud, that the nonuniformity in the intensity of emission across the region cannot be accounted for entirely by variable extinction, and that the vibrational and rotational levels are populated according to a Boltzmann distribution at a temperature of approximately 2000 K. Observations of the S(1) line by Joyce et al. (1978a) with a spectral resolution of 45 km s^{-1} and a spatial resolution of 23" x 35" do not show any evidence of line broadening or velocity shift of the line with respect to the bulk of the CO in the molecular cloud. Another measurement of this line by Ogden et al. (1978) with a spectral resolution of 11 km s^{-1} and a spatial resolution of 10".6 x 10".6 can be fit by a Gaussian profile having a width of approximately 13 km s^{-1} and little or no shift with respect to the sharp CO line. Both measurements were made on the peak of the S(1) emission to the north of the Becklin-Neugebauer (BN) and Kleinmann-Low (KL) infrared sources.

Calculations to explain the H_2 excitation have been published by Hollenbach and Shull (1977), Kwan (1977), and London, McCray and Chu

(1977). All three papers favor a model in which the H_2 is excited by a shock front moving at a velocity between 8 and 24 km s^{-1}. According to Kwan and London et al., the velocity of the shock cannot be higher than 24 km s^{-1}; otherwise all the molecular hydrogen would be dissociated in going through the shock. A model in which the H_2 is excited by near-ultraviolet pumping of the Lyman and Werner bands and returns to the ground level by a cascade through the vibrational levels (Black and Dalgarno 1976) apparently is ruled out by the observed ratios of $v = 2-1$ and $v = 1-0$ lines (Gautier et al. 1976; Beckwith et al. 1979).

The present Letter describes observations of the velocity profile of the S(1) line and the variations of this profile across the region of H_2 emission. Detailed discussions of models of the H_2 emission in Orion and of their relation to the other components of the molecular cloud are reserved for a future paper.

II. OBSERVATIONS

All the observations presented in this Letter were made with a single-stage piezoelectrically scanned Fabry-Perot interferometer coupled to an InSb detector. A cooled variable filter with a resolution $\Delta\lambda/\lambda = 1.3\%$ provided low resolution filtering.

Most of the observations were made at the Cassegrain focus of the 2.5 meter reflector at Mt. Wilson on 1978 November 15-18 and December 13, with a resolution of 20 km s^{-1}. Additional observations used in the analysis of the data were made at the Cassegrain focus of the 1.5 meter reflector at Mt. Wilson on 1978 December 6-9 with a resolution of 200 km s^{-1}.

All of the spectra in Orion were measured with a circular diaphragm of 10" diameter. The chopping was done against a blackbody at ambient temperature. The interferometer was scanned over a little more than one order every 20 seconds and the data were fed to a signal averager. One measurement normally consisted of 32 sweeps, or 11 minutes of integration. Several such measurements usually were added together to give each final spectrum. Before and after each measurement, the spectrum of a helium lamp was recorded in a similar fashion, for wavelength calibration. The alignment of the interferometer plates was checked approximately every two hours by visual inspection of the green line of a Mercury lamp (λ5461 Å) and was found to be stable.

Because of the minimum of prefiltering used, it is possible to contaminate the line profile of H_2 by unrelated emission or absorption features in overlapping orders of the Fabry-Perot. The H_2 v = 1-0 S(1) line occurs, however, in a spectral region where it is isolated both from other lines emitted in Orion and from major telluric features. There are nonetheless some weak telluric lines present in the spectra taken in Orion. To remove these from the data, a spectrum of the sky has been subtracted from the spectra obtained in Orion, with the constraint that a telluric line visible at each end of the spectra be cancelled. The major features of the S(1) line profiles are not sensitive to details of the subtraction of the telluric lines.

The instrumental profile of the interferometer was obtained by measurement at low spectral resolution of the S(1) line in Orion and by measurements at high spectral resolution of the widths of a telluric

emission line and of a Krypton line from a laboratory lamp, both at wavelengths close to that of the S(1) line; all methods give results consistent with an instrumental full width at half maximum of 17 km s^{-1}. Because of imperfections in the addition of the many scans that form each spectrum and slight misalignments of the plates during the course of the observations, the final resolution is approximately 20 km s^{-1}.

III. RESULTS

The observed spectra are shown in Figure 1, all plotted with the same arbitrary intensity scale. The uncertainty in the absolute calibration of the velocity scale is estimated at ± 5 km s^{-1} and relative velocities should be correct to ± 2 km s^{-1}. The positions of the spectra presented in Figure 1 are indicated in Figure 2 on the 13" map of Beckwith et al. (1978). The relative integrated intensities of the spectra are generally consistent with the 13" and 5" maps of these authors.

Visual inspection of the spectra of Figure 1 reveals the main result of the observations: the emission lines are very broad in the south-central portion of the H_2 map, near the BN and KL infrared sources, and are narrower but still significantly broadened outside of that region. The very broad lines (spectra 9, 10, 12, 13) have intrinsic widths at half maximum in the range of 37 to 58 km s^{-1}. They are asymmetric about the velocity of their peak spectral intensity in the sense that they have extended blue wings. In the case of the broadest line (spectrum 9) this wing extends approximately 100 km s^{-1} from the

peak of the line. The narrower lines have intrinsic widths at half maximum in the range of 18 to 32 km s^{-1} and they are substantially more symmetric with respect to the velocity of their peak spectral intensity. It is striking that the velocities of the peak spectral intensity of these narrower lines, which were observed at several well-separated positions, are the same at v_{LSR} = 13 km s^{-1} within the experimental uncertainty.

The red wings of the lines at all the positions measured coincide closely in velocity; the dispersion of the velocity at half the peak intensity is only 3 km s^{-1}, while the full widths at half maximum range from 18 to 58 km s^{-1}. The observed S(1) line emission can be described therefore as being composed of a blue and a red component, which are not necessarily discrete. The strength of the blue component is maximum in the region of positions 9, 10, 12, 13. The ratio of the strength of the red component to that of the blue component is smallest at position 12 and increases with distance from that position in all directions where observations have been made. The strength of the red component itself is observed to have a maximum approximately 25" from position 12, in several of these directions.

The present results are in some disagreement with the interpretation of Joyce et al. (1978a) and Ogden et al. (1978) that their data are due to rather narrow spectral features. It appears, however, that their data are consistent to within their noise levels with the line profiles reported here. Recently Smith et al. (1979) have observed a broad S(1) emission line near the position corresponding to spectrum 9 in this paper.

IV. DISCUSSION

Despite the incomplete spatial coverage of the S(1) line emission a number of conclusions may be inferred from the present observations. These relate to the motion of the emitting gas, the location and shape of the emitting region, the association of the observed H_2 with previously observed molecules and the physical processes responsible for the emission.

The somewhat organized appearance of the spatial variations of the S(1) line profiles argues that they are largely due to systematic rather than turbulent motions. An expansion about a center near BN and KL appears most consistent with the observed presence of broad lines whose centers are blueshifted with respect to those of the surrounding, narrower lines. Collapse appears unlikely since it is difficult to reconcile with the presence of blue wings and absence of red wings on lines originating from a region located deep within the molecular cloud. Rotation is implausible since no axis can be found which is consistent with all of the observed spectra. Uniform motion of a sheet of gas is ruled out by the large velocity dispersion of the lines.

Assuming roughly spherical expansion, the central velocity, which is given by the velocity of peak line intensity at the edges of the cloud, is 13 km s^{-1} (LSR). This is close to the 9.0 km s^{-1} velocity of the extended molecular cloud as determined from numerous radio observations. Typical expansion velocities may be estimated from the velocities on the blue wings of the broad lines. A value of $\sim$ 40 km s^{-1} is obtained by using the velocity at half the maximum line intensity.

It is apparent, however, from the large range of blueshifted velocities that a differential expansion of the emitting cloud is occurring. The time since the expansion began, as estimated from the size of the emitting region and a velocity of 40 km s^{-1}, is approximately 2 x 10^3 years.

The position of the center of expansion should be located in the region containing the broadest lines, which is approximately along the line of sight to BN and KL. The extinctions to BN (Gillett et al. 1975; Joyce et al. 1978b; Hall et al. 1978) and to the region of molecular hydrogen emission (Beckwith et al. 1979: Simon et al. 1979) are similar. The significance of this result, however, is unclear because of the uncertainty in the amount of extinction directly associated with BN. The absence, near the proposed center of expansion, of a wing of S(1) emission at high redshift, is indicative either of heavy obscuration within the expanding region or of the absence of gas on the back side of the expanding region. A comparison of the extinction to the H_2 (Beckwith et al. 1979) and that for the entire cloud (Thaddeus et al. 1971) argues against the second alternative. For the first alternative to be consistent with the observations roughly two magnitudes of extinction at 2.12 microns are required within the expanding region. Assuming the ratio of visual to two micron extinction is 10 (van de Hulst 1946; Johnson 1968) and the ratio of gas to visual extinction is 2 x 10^{21} atom cm^{-2} mag^{-1} (Knapp et al. 1973), the average density required within the expanding cloud would be $\sim 10^5$ cm^{-3}. This is comparable to density estimates for the molecular cloud as a whole (Thaddeus et al. 1971; Liszt et al. 1974: Evans et al. 1975).

Two properties of the observed line profiles indicate that the S(1) emission originates either in many shells or in one shell whose thickness is a substantial fraction of the radius of the emitting region. First, the presence of broad lines implies a wide range of velocities for the emitting gas, which makes confinement of this gas to a single thin shell unlikely. Second, although at positions 6, 7, 8 and 14 there is evidence for limb brightening, such as would occur in the case of a thin shell, the region of emission extends well beyond the first three of these locations. Assuming a single shell of thickness 0.05 pc, and taking from Beckwith et al. (1979) the column density of excited $H_2 \sim 3 \times 10^{20}$ cm^{-2}, the volume density of H_2 is $\sim 2 \times 10^3$ cm^{-3}. This value is far below the estimates of the average density for the molecular cloud and the gas density within the expanding region, as shown earlier in this Letter. This indicates that if the S(1) emission comes from a single thick shell only a small fraction of the hydrogen in the shell is in molecular form.

The present results strongly support an association of the H_2 emission with the "plateau" source of broad molecular line emission at radio frequencies as suggested by Kwan and Scoville (1976). The position of the "plateau" source of CO, particularly as determined by the (3 → 2) transition (Phillips et al. 1977), and the location of the high velocity H_2O masers (Genzel and Downes 1977) are in good agreement with the location of the region emitting the broadest S(1) lines. The breadth of the S(1) line is as great or greater than the "plateau" source radio lines. In addition, the velocity of peak S(1)

line emission agrees with the estimated central velocities of the "plateau" source lines.

The radio lines from the "plateau" source are approximately symmetric about the central velocity whereas the S(1) line has no extended redshifted wing. This difference can be explained by the presence of dust within an expanding region, as suggested earlier. Rotation and collapse have been rejected as the cause of the broad lines of the "plateau" source, both on observational grounds (Kwan and Scoville 1976) and by dynamical arguments (Zuckerman et al. 1976; Genzel and Downes 1977). Kwan and Scoville concluded that the source is undergoing differential expansion, a conclusion also reached in this Letter.

An interesting trend in the "plateau" source emission of CO (2 → 1) (Wannier and Phillips 1977), CO (3 → 2) (Phillips et al. 1977), SO (Wannier and Phillips 1977), SO_2 (Snyder et al. 1975), SiO (Dickinson 1972; Lada et al. 1978), HCO^+ (Turner and Thaddeus 1977) and OCS (Lada et al. 1978) is that the full widths at half maximum of the observed lines are smaller for those lines which peak further north of KL. This trend appears to parallel that seen in the S(1) line, after accounting for differences in spatial resolution. Lada et al. have suggested links between the chemistry of a shocked gas and the abundances and locations of "plateau" source molecules in the gas. Further spectral observations of the 2.0 to 2.5 μm lines of H_2, which are possible at higher spatial resolution than has been used for the radio lines, may provide sufficiently detailed information about the emitting gas to test their hypotheses.

The results presented in this Letter place several constraints on the physical processes responsible for the excitation and expansion of H_2 in Orion. Both the wide range of velocities observed and the size and shape of the emitting region implied by the observations preclude a single shock front moving at a low enough velocity ($v < 24$ km s^{-1}) to collisionally excite but not dissociate the H_2. Nevertheless the case for collisional excitation remains strong. Indeed the present estimate of the amount of extinction inside the region of H_2 emission strengthens the argument of Beckwith et al. (1979) that no single stellar source of ultraviolet radiation either inside or outside of the cloud can account for more than a small fraction of the excitation of the H_2.

The conclusions presented in this section are largely independent of gas density and extinction variations across the region of H_2 emission. Both may be responsible for much of the spatial fluctuation of the observed S(1) line intensity. Additional observations are necessary to assess the importance of these effects and provide more sensitive tests of the physical processes at play in the Orion molecular cloud.

V. SUMMARY

The observations of the velocity profiles of the S(1) line in Orion show that:

(1) The full widths at half maximum of the observed S(1) lines vary between 18 and 58 km s^{-1}.

(2) A small fraction of the observed H_2 gas is moving at a velocity of approximately -100 km s^{-1} with respect to the bulk of the molecular cloud.

(3) The region of emission is probably undergoing differential expansion from a center roughly along the line of sight to the BN-KL infrared sources.

(4) The H_2 emission is probably associated with the "plateau" source seen in the emission of other molecules.

(5) Although collisional excitation is the likely cause of the S(1) emission, the excitation is not produced by a single shock front moving at low velocity ($v < 24$ km s^{-1}) through the molecular cloud.

ACKNOWLEDGMENTS

We thank V. Stephensen and M. Kriegel for their assistance in constructing the instrument. We are grateful to D. Carr, J. Frazier and H. Lanning for assistance with the observations and to the staff of the Mt. Wilson Observatory for their efficient cooperation. We also thank J. Kristian for the loan of the data acquisition instruments. These measurements would not have been possible without the excellent InSb detector system developed and optimized by K. Matthews and S. E. Persson. We gratefully acknowledge G. Neugebauer, S. E. Persson and B. T. Soifer for many useful comments and suggestions, G. Forrester for technical assistance, and S. Hage and J. Boyer for help with the manuscript. This work was supported by NSF grants AST77-20516 and AST78-16826 and NASA grants NGL 05-002-207 and NGL 05-002-140. D. Nadeau is a fellow of the National Research Council of Canada.

REFERENCES

Beckwith, S., Persson, S. E., Neugebauer, G., and Becklin, E. E. 1978, Ap. J., 223, 464.

Beckwith, S., Persson, S. E., and Neugebauer, G. 1979, Ap. J., 227, in press.

Black, J. H., and Dalgarno, A. 1976, Ap. J., 203, 132.

Dickinson, D. F. 1972, Ap. J. (Letters), 175, L43.

Evans, N. J., II, Zuckerman, B., Sato, T., and Morris, G. 1975, Ap. J., 199, 383.

Gautier, T. N., III, Fink, U., Treffers, R. P., and Larson, H. P. 1976, Ap. J. (Letters), 207, L129.

Genzel, R., and Downes, D. 1977, Astr. Ap., 61, 117.

Gillett, F. C., Jones, T. W., Merrill, K. M., and Stein, W. A. 1975, Astr. Ap., 45, 77.

Grasdalen, G. L., and Joyce, R. R. 1976, Bull. A.A.S., 8, 349.

Hall, D. N. B., Kleinmann, S. G., Ridgway, S. T., and Gillett, F. C. 1978, Ap. J. (Letters), 223, L47.

Hollenbach, D. J., and Shull, J. M. 1977, Ap. J., 216, 419.

Johnson, H. L. 1968, in Nebulae and Interstellar Matter, eds. B. M. Middlehurst and L. H. Aller (Chicago: University of Chicago Press), p. 167.

Joyce, R. R., Gezari, D. Y., Scoville, N. Z., and Furenlid, I. 1978a, Ap. J. (Letters), 219, L29.

Joyce, R. R., Simon, M., and Simon, T. 1978b, Ap. J., 220, 156.

Knapp., G. R., Kerr, F. J., and Rose, W. K. 1973, Ap. Letters, 14, 187.

Kwan, J. 1977, Ap. J., 216, 713.

Kwan, J., and Scoville, N. 1976, Ap. J. (Letters), 210, L39.

Lada, C. J., Oppenheimer, M., and Hartquist, T. W. 1978, Ap. J. (Letters), 226, L153.

Liszt, H. S., Wilson, R. W., Penzias, A. A., Jefferts, K. B., Wannier, P. G., and Solomon, P. M. 1974, Ap. J., 190, 557.

London, R., McCray, R., and Chu, S. I. 1977, Ap. J., 217, 442.

Ogden, P. M., Roesler, F. L., Reynolds, R. J., Scherb, F., Larson, H. P., Smith, H. A., Daehler, M. 1978, Ap. J. (Letters), 226, L91.

Phillips, T. G., Huggins, P. J., Neugebauer, G., and Werner, M. W. 1977, Ap. J. (Letters), 217, L161.

Simon, M., Righini-Cohen, G., Joyce, R. R., and Simon, T. 1979, preprint.

Smith, H. A., Fink, U., Larson, H. P., Feierberg, M., Ogden, P. M., Roesler, F. L., Reynolds, R. J., and Scherb, F. 1979, talk presented at the 153rd meeting of the A.A.S., Mexico City, 1979.

Snyder, L. E., Hollis, J. M., Ulich, B. L., Lovas, F. J., Johnson, D. R., and Buhl, D. 1975, Ap. J. (Letters), 198, L81.

Thaddeus, P., Wilson, R. W., Kutner, M., Penzias, A. A., and Jefferts, K. B. 1971, Ap. J. (Letters), 168, L59.

Turner, B. E., and Thaddeus, P. 1977, Ap. J., 211, 755.

van de Hulst, H. C. 1946, Recherches Astronomiques de l'Observatoire d' Utrecht, 11, part 1.

Wannier, P. G., and Phillips, T. G. 1977, Ap. J., 215, 796.

Zuckerman, B., Kuiper, T. B. H., and Kuiper, E. N. R. 1976, Ap. J. (Letters), 209, L137.

FIGURE CAPTIONS

Figure 1. Spectra of the H_2 v = 1-0 S(1) line in Orion after sky subtraction. The spectral resolution is 20 km s^{-1}. The numbers on the left-hand side of the spectra refer to the corresponding positions in Figure 2. The relative intensities of the lines of different spectra are accurate to 10%. The uncertainty on the calibration of the origin of the velocity scale is ± 5 km s^{-1} and the relative velocities of the lines of different spectra are accurate to ± 2 km s^{-1}. The noise level should be judged from each baseline individually, as different integration times were used on different spectra. The interval between -15 and 0 km s^{-1} in spectrum 12 has been fitted with a straight line consistent with two of the three measurements averaged in this spectrum, the third one having an extraneous spike.

Figure 2. The positions of the spectra presented in Figure 1 are shown on the 13" map of the H_2 v = 1-0 S(1) line emission from Beckwith et al. (1978). The size of the circles corresponds to the 10" spatial resolution used in the measurements. Pointing uncertainties are typically ± 3".

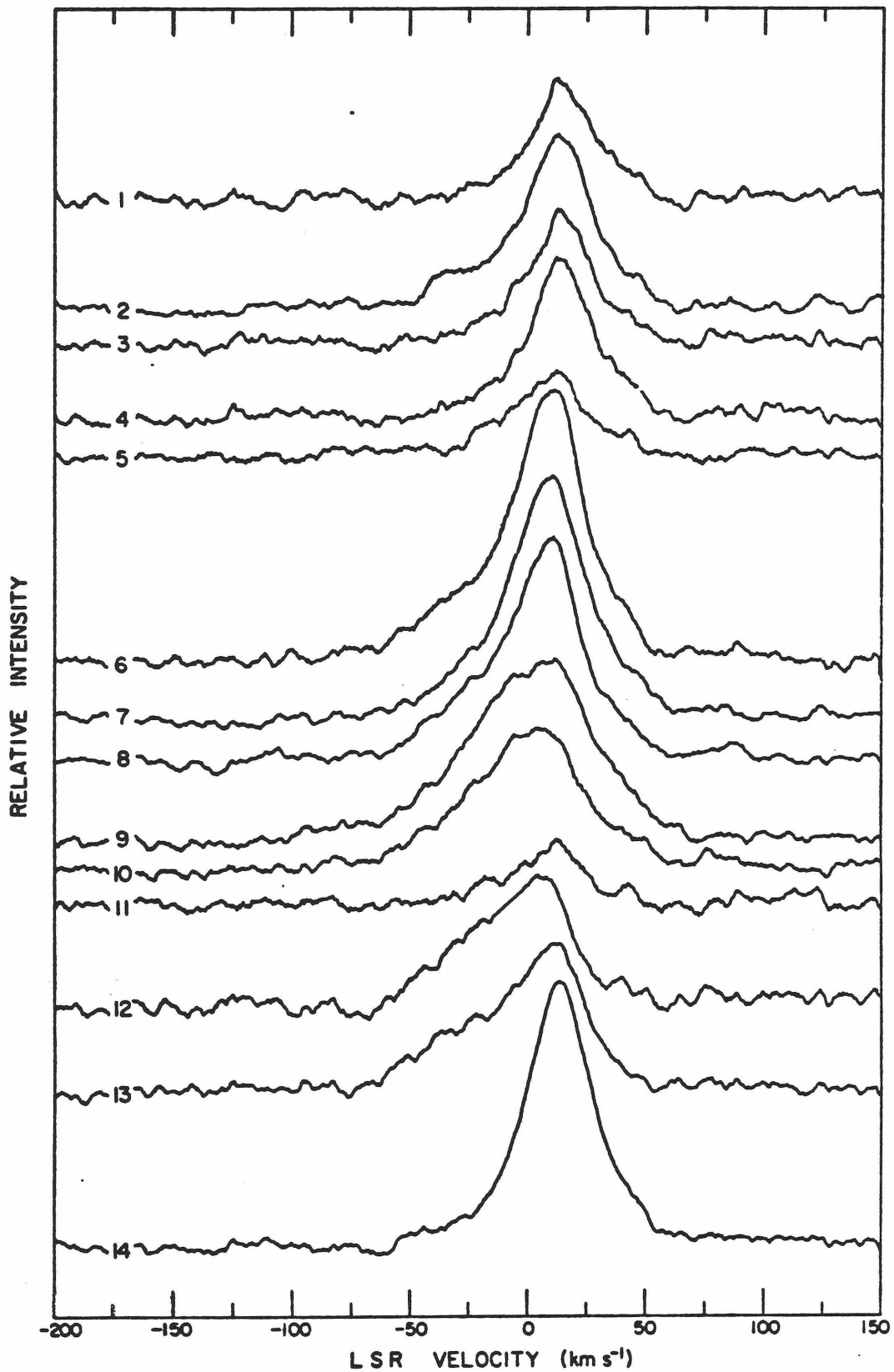
RELATIVE INTENSITY
1
2
3
4
5
6
7
8
9
10
11
12
13
14
-200
-150
-100
-50
0
50
100
150
LSR VELOCITY (km s⁻¹)

Figure 1

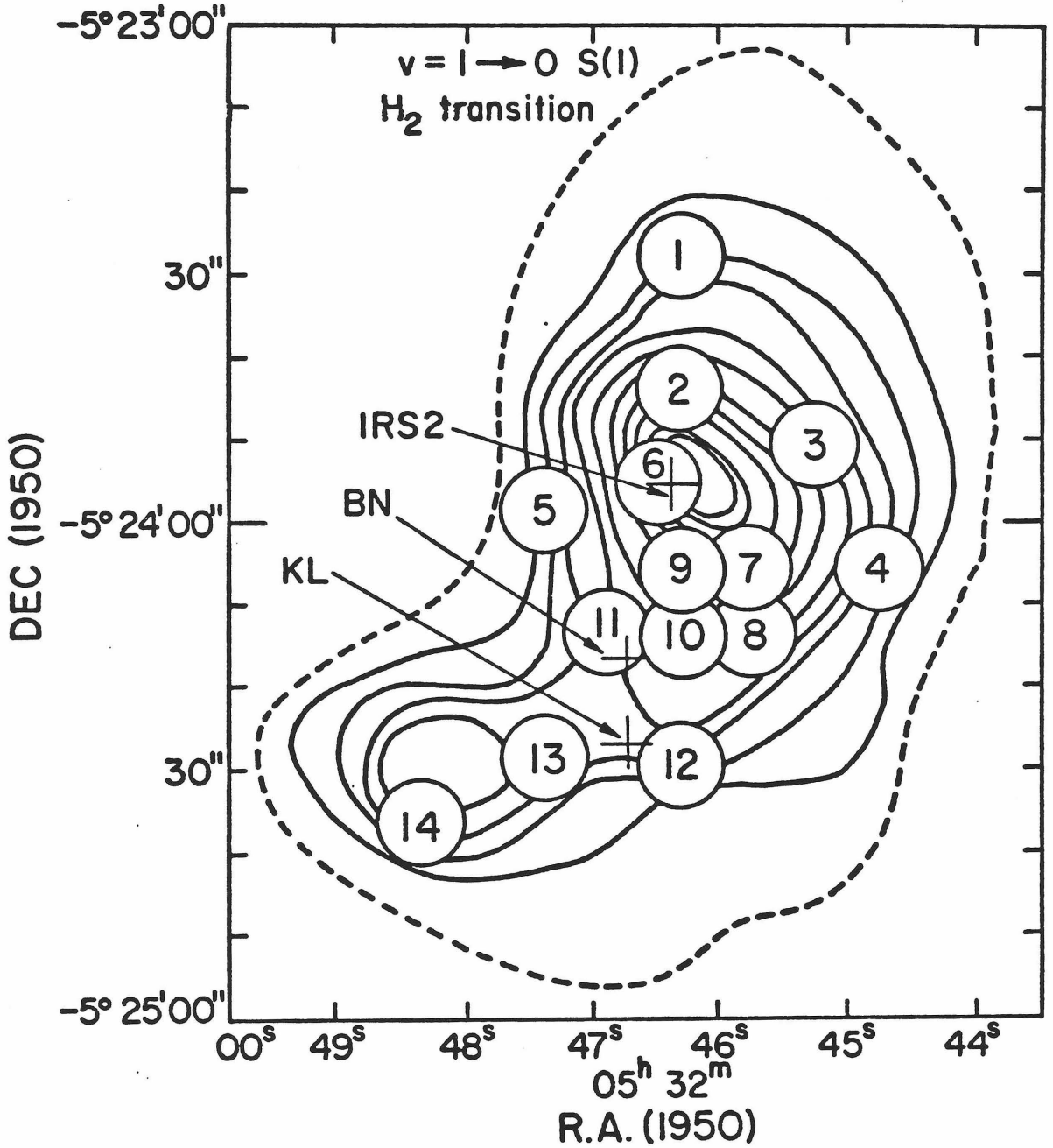
v = 1 → 0 S(1)
H2 transition
-5°23'00"
30"
-5°24'00"
30"
-5°25'00"
DEC (1950)
IRS2
BN
KL
1
2
3
4
5
6
7
8
9
10
11
12
13
14
00s
49s
48s
47s
46s
45s
44s
05h 32m
R.A. (1950)

Figure 2

PAPER II:

THE MOTION AND DISTRIBUTION OF THE VIBRATIONALLY EXCITED H_2 IN THE ORION MOLECULAR CLOUD

To be submitted to the *Astrophysical Journal*

In collaboration with

G. Neugebauer and T. R. Geballe

ABSTRACT

Observations of line profiles of the vibrationally excited H_2 gas in the Orion molecular cloud are presented. The $v=1\rightarrow 0\ S(1)$, $v=1\rightarrow 0\ S(0)$ and $v=2\rightarrow 1\ S(1)$ lines, emitted at a wavelength near $2\,\mu$m, have been observed with a spectral resolution of $20\,\mathrm{km\,s^{-1}}$. The region has been mapped extensively in the $v=1\rightarrow 0\ S(1)$ line with a spatial resolution of 10" and 5", and the line has been monitored at a few positions over a period of 15 months. The profiles of the $v=1\rightarrow 0\ S(0)$ and $v=2\rightarrow 1\ S(1)$ lines have been compared at two positions. The mapping measurements show variations from the periphery where the profiles are narrow, symmetric and have a peak velocity equal to that of the molecular cloud, to the center of the region of emission where the profiles are wide, asymmetric and blueshifted. The line profiles do not appear to vary with time or with the energy of the upper level of the transition. The results are interpreted by a model of a radially expanding flow of gas. From a study of H_2 excitation behind a shock front and in a magnetic precursor ahead of a shock wave, it is concluded that the high velocity emission comes from the high velocity gas in the flow, and the low velocity emission comes from gas in the molecular cloud surrounding the flow, with density inhomogeneities contributing to the detailed profiles. Finally the H_2 emission is compared to the CO and H_2O maser emission and to the infrared continuum sources.

Subject headings: infrared: spectra – interstellar: molecules – line profiles – molecular processes – nebulae: Orion Nebula

I. INTRODUCTION.

The region of the infrared cluster in Orion is one of the best observed molecular cloud regions and a wealth of information is associated with it. It now appears that most of the phenomena observed in the direction of this region are interrelated, and it is becoming possible to make models which describe this interrelation. Since the infrared cluster is believed to be the site of recent star formation, these models may provide some information on this process, which is as yet very poorly understood.

Molecular hydrogen is the most abundant constituent of molecular clouds (Spitzer 1978), but due to the high energy of both its vibrational and rotational levels and its lack of a dipole moment, it is observed only in a small fraction of the known molecular clouds. Indeed the discovery, by Gautier *et al.* (1976), of strong interstellar H_2 emission from vibrationally excited levels has prompted many new studies of energetic phenomena in molecular clouds. Since the initial discovery, the measurements of Beckwith *et al.* (1979, hereafter BPN) and Simon *et al.* (1979, hereafter SRJS) have shown that the H_2 gas observed at $2\,\mu$m in Orion, has a temperature $T \approx 2000\,$K and a total luminosity $L \approx 2000\,L_\odot$. Comparison of the observations with theoretical calculations (Hollenbach & Shull 1977, Kwan 1977, London *et al.* 1977) indicated that shock waves were probably responsible for the excitation of H_2.

Following these results, spectroscopic measurements of the $v=1\rightarrow 0\,S(1)$ line in Orion by Nadeau & Geballe (1979, hereafter PaperI) and Nadeau *et al.* (1980) showed that: a) the line shows large variations in spectral width with position, is emitted with large blueshifts in many locations, and in a few cases extends up to a velocity of $-100\,\mathrm{km\,s^{-1}}$, b) the emission region is probably undergoing differential expansion from a center roughly along the line of sight

to the Becklin-Neugebauer and Kleinmann-Low infrared sources, and c) although collisional excitation is the likely cause of the H_2 emission, the excitation is not produced by a single shock front moving at low velocity ($V < 24\,km\,s^{-1}$) through the molecular cloud.

The observed high velocities raise a problem since the theoretical calculations have shown that all the hydrogen molecules going through a shock with a velocity higher than $24\,km\,s^{-1}$ are dissociated and would need to reform if they are to be observed behind the shock. Many recent studies have addressed this problem (Dalgarno & Roberge 1979, Hollenbach & McKee 1980, Chevalier 1980, Draine 1979) but none of the existing models of the excitation of H_2 is yet entirely satisfactory. Understanding the detailed excitation mechanism is important for the study of the chemical evolution of the molecular cloud (Iglesias & Silk 1978, Elitzur 1979), the nature of the infrared sources (Downes *et al.* 1980, Genzel *et al.* 1980), and the role of magnetic fields in molecular clouds (Draine 1980).

The measurements presented here, which include the data published in Paper I, confirm the conclusions reached in Paper I, and permit a more thorough description of the motions of H_2 throughout the emission region. The following discussion attempts to determine the morphology of the emission region, the detailed H_2 excitation process, and the relation of H_2 to other observed sources of continuum radiation and molecular line emission.

II. OBSERVATIONS.

All the observations were high resolution spectroscopic measurements made with a single-stage, piezoelectrically scanned, Fabry-Pérot interferometer coupled to an InSb detector. A cooled variable filter with a resolution

$\Delta\lambda/\lambda = 1.3\%$ provided low-resolution filtering. The instrumental full spectral width at half maximum was $20 \pm 2\,km\,s^{-1}$. A more detailed description of the instrument is given in the Appendix.

The observations were made at the 2.5 m telescope of Mt.-Wilson Observatory and the 5 m telescope of Palomar Observatory. A journal of the observations is given in Table 1. At all times, the seeing disk was substantially smaller than the size of the diaphragm used. The observational technique consisted of scanning a portion of the spectrum equivalent to a $350\,km\,s^{-1}$ velocity interval ($700\,km\,s^{-1}$ for the $40\,km\,s^{-1}$ resolution measurements), every 20 seconds for a period of 11 minutes. This technique is the same as that described in Paper I, except for the following modifications: after 1979 February, a line from a Krypton lamp (λ2.1165471), rather than Helium (λ2.113203), was used for wavelength calibration, and in 1980 February, chopping was done at 10 Hz against a region of the sky situated alternately 45" east or west of the source, rather than against a blackbody at ambient temperature.

The velocity calibration technique has been improved (see Appendix) compared to that of Paper I and the results described in Paper I have been corrected slightly. The velocity scale for each spectrum should be accurate to better than 1%, the uncertainty in the absolute calibration is $\pm 3\,km\,s^{-1}$, and the uncertainty in the relative calibration between spectra is $\pm 2\,km\,s^{-1}$. No absolute intensity calibration was attempted; in general, a single intensity measurement was made at the beginning of the night to check the sensitivity of the detector. Since the measurements are relatively insensitive to slow variations of the transparency of the atmosphere, they were sometimes made in weather of less than photometric quality.

The observations were of three sorts: a) a mapping of the region of emission with a 10" diaphragm and partial mapping with a 5" diaphragm, b) a comparison of the spectral profiles of the $v=1\rightarrow 0$ $S(0)$ and of the $v=2\rightarrow 1$ $S(1)$ lines, and c) a monitoring over a 15-month period of the $v=1\rightarrow 0$ $S(1)$ line at three positions.

III. RESULTS.

Two conventions are adopted throughout this paper. All velocities are measured with respect to the velocity of the molecular cloud, that is $V = V_{LSR} - 9\,\mathrm{km\ s^{-1}}$ (see *e.g.* Zuckerman *et al.* 1976), and all spectra and other features of the region of emission that are not directly associated with compact infrared sources are designated by their position at epoch 1950.0, less the constant part ($5^h\,32^m, -5°$). The positions and nomenclature of the compact infrared sources are taken from the 20 μm continuum measurements of Downes *et al.* (1980).

a) Mapping measurements.

Most of the data come from the mapping of the region of emission. These are presented a) in the form of a map of the spectra obtained with a 10" diaphragm (the 10" map) and a map of the spectra obtained with a 5" diaphragm (the 5" map), and b) in the form of maps showing the spatial distribution of the emission for various velocity ranges. The former maps emphasize the precise profiles of individual spectra, while the latter emphasize the spatial structure of the region.

The 10" map is shown in Figure 1 and the 5" map in Figure 2; the latter covers a small portion of the former, indicated by a dashed contour in Figure 1. In both cases all the spectra are plotted with the same peak-to-baseline amplitude.

The spectra are plotted between the velocities of −122 and +66 km s^{-1}, but the full extent of the measured spectrum (~ 350 km s^{-1}) was used to determine the baseline. The smoothing due to the instrumental profile has not been removed; this profile is shown on both figures, and features which are sharp with respect to it indicate the noise level.

The data shown in Figures 1 and 2 were used to produce the maps of Figure 3. Plotted in the latter is the fraction of the energy received within a 20 km s^{-1} interval (30 km s^{-1} for Figure 3e), in the range from −120 to +70 km s^{-1}. The data are plotted on a non-linear scale to emphasize the low level signals at high velocity, and the same scaling is used in all the maps. The area sampled in each map is the same, but whenever a region emits less than 1% of its energy in a given velocity range, this region is left blank on the corresponding map. The maps in Figure 3 are meaningful in describing general areas where the data from many regions agree in their characteristics; they should not be interpreted as statements about individual regions since local variations are due in part to low signal-to-noise.

The main result of the mapping of the line profiles is the identification, on the basis of their observed spectra, of two regions (*cf.* Figures 1 and 2). The central region is characterized by profiles with extended wings at negative velocities, while the peripheral region, which surrounds it, is characterized by narrow profiles centered at $V = 0$. The spectral characteristics of each of these regions are discussed in the next two sections.

i) The Central Region.

The central region is defined as that region where the line profiles are broad and emission is seen mostly at negative velocities. This region is further

divided into two parts, mainly on the basis of measurements of the infrared continuum and of molecular line emission at radio wavelengths, but also on the basis of distinctions inherent to the H_2 data. The true central part, where most of the infrared sources and the molecular masers are concentrated, is centered approximately at (46.5,−24 15) and extends over ~ 35" in declination and ~ 30" in right ascension (*cf.* Figures 1 and 3b,c,d). All further references to the central region apply specifically to this central part. The northern part extends directly to the north of the true central part, approximately from (46.3,−24 10) to (46.3,−23 45). The intensity of the H_2 lines is much higher in the northern part than in the central one, and the most extreme velocities at which H_2 emission is observed are seen in a region ~ 15" north of the center (Figure 3a,e). At a distance of 480 pc (Downes *et al.* 1980), the diameter of the region of high velocity emission is $\sim 2.5 \times 10^{17}$ cm.

An average profile was obtained by adding together the spectra in the central region after normalizing them to a uniform peak amplitude. The high signal-to-noise ratio obtained made it possible to remove from this average profile the smoothing effect of the instrumental profile. An approximate input function was determined from visual comparison of these two profiles, and improved by successive comparisons of the observed profile with the convolution of the input function and the instrumental profile. A good fit to the observed profile was obtained after a few iterations; this input function is shown in Figure 4. The peak of emission of the average profile is at a velocity of -6 ± 3 km s^{-1}. The drop on the positive velocity side is very fast, and the intensity is less than 10% of the peak value past a velocity of +15 km s^{-1}. On the negative velocity side the profile extends to a velocity of −80 km s^{-1}, with a noticeable change of slope at a velocity of ~ −27 km s^{-1}. The procedure used to remove the effect of the

instrumental profile results in uncertainties of $\sim 5\,\mathrm{km\ s^{-1}}$ for features such as the velocity at which the change of slope occurs.

The spectra from the northern part of the region were also added together, mainly for the purpose of finding the full velocity extent of the H_2 emission. In order to improve the signal-to-noise ratio as much as possible the spectra were added with a weight proportional to the integration time. No other selection criteria were applied and the spectra from a large region were used; it is therefore improbable that a feature due to the noise has been inadvertently enhanced. The weighted average position of the resulting spectrum is approximately (46.2,−24 00). The same iterative procedure as outlined above was used to remove the effect of the instrumental profile from the average spectrum, and the resulting input profile is shown in Figure 5. Emission definitely is present at a velocity of $-100\,\mathrm{km\ s^{-1}}$ and possibly at a velocity as extreme as $-120\,\mathrm{km\ s^{-1}}$. At positive velocities the signal is very weak beyond a velocity of $+30\,\mathrm{km\ s^{-1}}$ and uncertainties in the baseline make it hard to find the maximum extent of the profile; there seems to be emission up to a velocity of $+60\,\mathrm{km\ s^{-1}}$.

ii) The Peripheral Region.

The line profiles in the peripheral region are broader than the instrumental profile but much narrower than the profiles in the central region, and are mostly symmetric. In the peripheral region, the peak brightness of the profiles is at $V = 0$ (*cf.* Figures 1, 3d), and a comparison of the lines measured at the outermost positions, in every direction except directly east of the central region, shows no variation from this velocity outside of the $2\,\mathrm{km\ s^{-1}}$ uncertainty. The profile observed in the southeast at (48.3,−24 36), which has a very high signal-to-noise ratio, is approximated very well by the convolution of the instrumental profile with a Gaussian of full width at half maximum $\mathrm{FWHM} = 22 \pm 2\,\mathrm{km\ s^{-1}}$,

where the uncertainty is mainly due to the uncertainty in the width of the instrumental profile. The FWHM of the other spectra at the periphery has a dispersion of $\pm$ 3 km s^{-1} around the width at (48.3,−24 36).

iii) Intensities.

As mentioned in II., the measurements do not provide an accurate value of the absolute intensity. In some cases, however, the measurements have been made in a way that enables a comparison of the peak intensity of nearby spectra.

Measurements to the south, to the west, to the north and to the northeast show a general pattern in which the emission peaks are brighter at the periphery than at positions closer to the center. To the northwest, there is a maximum of peak brightness in a region $\sim$ 15" in diameter, centered approximately at (45.5,−24 08). This region is somewhat distant from the boundary of the emission region in that direction, and while in most directions the brightest peak has $V = 0$, to the northwest the region of brightest peak emission has $V \approx -4$ km s^{-1}. There is no increase in brightness to the southwest and to the east; in these directions the data of Beckwith *et al.* (1978, hereafter BPNB) show a very rapid decrease in intensity (see the contours of Figure 1).

There is a good agreement between the data of BPNB and the relative integrated intensities obtained from the high spectral resolution measurements. In particular, the local maxima labeled Pk 2 and Pk 5 by BPNB correspond to maxima of the peak brightness in the present data. (*cf.* Figures 1 and 2) On the other hand, the local maximum labeled Pk 1 by BPNB does not correspond to a brighter peak but to a wider line. Finally, the position of a dip in intensity between the continuum sources IRc1 and IRc2, found by BPNB, corresponds to

the position of the line profile with the largest observed width at half maximum (97 km s^{-1}) of all the spectra measured (*cf.* Figure 1). This line has a peak brightness substantially lower than the peak brightness of the lines measured at adjacent positions to the south and to the west.

b) Comparison of the $v=1\rightarrow 0$ S(0) and $v=2\rightarrow 1$ S(1) Line Profiles.

The $v=1\rightarrow 0$ S(0) line, emitted at $\lambda = 2.223\,\mu$m from an upper level with $E/k = 6470$ K, and the $v=2\rightarrow 1$ S(1) line, emitted at $\lambda = 2.247\,\mu$m from an upper level with $E/k = 12550$ K, were measured first on 1979 February 10 and again on 1980 February 5-6 at the Palomar 5 m telescope. Since the difference in the upper level energies of the two transitions is large with respect to the 2000 K excitation temperature, any difference in the profiles should be a sensitive indicator of temperature variation in the regions of vibration-rotation emission. Since the wavelengths of the lines are very close, there should be little effect from possible variations of the extinction.

The accuracy of the comparison is limited by the signal-to-noise which was obtained. The measurements of 1979 were made with a spectral resolution of 40 km s^{-1}. Even after smoothing over a velocity interval of 35 km s^{-1}, only the data at position (48.3,−24 36) have a high enough signal-to-noise ratio to be significant. In 1980, all the observations were made at position (46.3,−24 06), with a spectral resolution of 20 km s^{-1}, and the line profiles obtained have a much higher signal-to-noise.

The results are shown in Figure 6; the profiles of both lines are very similar. There is thus no evidence of a correlation between the velocity and the temperature of the gas in the regions of vibrationally excited H_2. The signal-to-noise of the data of 1980 is such that if, for example, the gas moving at

$-40 < V < 0$ km s^{-1} were at $T = 2000$ K, it would be possible to detect a change of $\sim \pm 500$ K in the temperature of the gas at $-80 < V < -40$ km s^{-1}.

c) Monitoring of the Line Profiles

The line profile of the $v=1 \rightarrow 0$ $S(1)$ transition was measured repeatedly at positions (46.3,−24 06), (48.3,−24 36) and (46.6,−24 29), during the 15-month period from 1978 November to 1980 February. In particular, measurements of the profile at (46.6,−24 29) were made both before and soon after one of the H_2O masers at this position increased in intensity by three orders of magnitude (Abraham *et al.* 1979). The measurements have shown no variation of the profiles which cannot be accounted for by variations in the resolution used, by differences in the pointing, or by noise fluctuations.

These results are in contrast with those of Ogden *et al.* (1979), who have reported that the profiles of the $v=1 \rightarrow 0$ $S(1)$ line near position (46.3,−24 06) varied from a width of 13 ± 4 km s^{-1} and a peak velocity of 0.3 km s^{-1} to a width of 45 ± 7 km s^{-1} and a peak velocity of -9 km s^{-1} in the 10-month period between February and October 1978. If such variations had occurred over the period of the observations reported here, they would have been easily detected.

IV. DISCUSSION.

The main results from the previous section are that a) the 2 μm H_2 emission region has a rough circular symmetry, with broad lines emitted at negative velocities in the central part, and narrower lines centered at $V = 0$ at the periphery, b) there is emission at velocities up to -100 km s^{-1}, but the peak emission is always between -6 km s^{-1} and 0, and c) in general the peak emission becomes brighter at the periphery. Two other important characteristics of the excited H_2

gas are its temperature, $T \approx 2000\,K$, and its total luminosity, $L \approx 2000 L_{\odot}$ (BPN, SRJS).

The following discussion is in four parts. In section a) the rough circular symmetry of the H_2 emission region is interpreted as arising from a flow of gas that originates from a central source in the infrared cluster, and expands almost freely until it reaches a radius of a few times $10^{17}\,cm$ ($\sim 30''$), where it encounters dense material from the surrounding molecular cloud. The brightening of the peak emission at the periphery suggests that interaction between the flow and the molecular cloud, at the boundary of the expansion region, contributes to the H_2 emission.

This hypothesis of interaction between the flow and the quiescent cloud, together with the observations of high velocity emission, lead, in section b), to the study of two models which have been proposed for the excitation mechanism: heating behind a shock front, and heating in a magnetic precursor ahead of a shock front. Strong constraints are put on both models by the high temperature and luminosity of H_2, but in both cases some questions remain unanswered.

In section c), the observation of emission over a velocity range from 0 to $-100\,km\,s^{-1}$ is interpreted in view of the conclusions of the two previous sections. Density inhomogeneities are probably an important characteristic of the region of emission and some observational evidence of density inhomogeneities is presented.

Understanding the relationship between the various molecular and continuum data is an important step toward a complete explanation of the phenomena evolving inside the molecular cloud. In section d) an attempt is made to relate the H_2 data to the CO and H_2O maser data, and to the continuum infrared sources.

a) Radial Expansion and Shell Emission.

The profiles of the H_2 lines shown in Figures 1 and 2 are probably due mostly to actual motion of the emitting gas rather than scattering off fast moving grains, since the $v=0\rightarrow 0$ $S(2)$ line of H_2 at 12.3 μm, which should be much less sensitive to scattering than the 2 μm lines, also shows the large line widths measured at 2 μm (Beck *et al.* 1979, S. Beck, p.c.). On the other hand, thermal broadening at a temperature of 2000 K would account only for a FWHM = 7 km s^{-1}, and turbulence alone would cause the profiles to be symmetric with respect to the velocity of the molecular cloud.

The spatial distribution of the line profiles in the emission region suggests systematic motion of the molecular hydrogen, and we interpret the difference between the line profiles observed in the central region and in the peripheral region as meaning not that these regions are physically different, but rather that they show different perspectives of one global motion. The similarity of the velocities measured all around the region of emission (III.a.*ii*) imply that any global rotation of the mass of gas is a negligible contributor to the H_2 line profiles measured.

The spatial extent of the high velocity ($|V| > 10$ km s^{-1}) CO $J=2\rightarrow 1$ emission (Knapp *et al.* 1980) is shown in Figure 3 as a circle 40" in diameter. The center of the circle has been made to coincide with the center of the high velocity CO $J=3\rightarrow 2$ emission, (46.7,−24 19) (Phillips *et al.* 1977), because the absolute position of the measurements of Knapp *et al.* has a large uncertainty. Figure 3 shows that the CO emission is essentially coincident with the central region of H_2 emission. In addition the measurements of the $J=2\rightarrow 1$ transition show that CO is moving at velocities up to $\sim \pm 95$ km s^{-1}, which, at negative velocities, is similar to the extreme velocities seen in H_2. This agreement suggests that H_2

and CO are accelerated by the same process. The CO emission observed at positive velocities, however, has no counterpart in the H_2 line profiles. The symmetry of the CO profile and the asymmetry of the H_2 profile can probably best be explained by spherical expansion of a dusty region, where the emission from the H_2 gas moving at more positive velocities suffers a larger extinction (*see* Paper I).

The amount of differential extinction at 2.1 μm required between the gas moving at negative and positive velocities to explain the observed line profiles of H_2 is roughly 3 mag.. From measurements of the column density of ^{13}CO (Hall *et al.* 1978) and ^{12}CO (Phillips *et al.* 1977), and from estimates of the mass of expanding gas (Scoville 1980, Knapp *et al.* 1980), values of the visual extinction across the expanding sphere ranging from 10 to 100 mag. are obtained, depending on the assumptions concerning the $^{12}CO/^{13}CO$ abundance ratio, the CO/H_2 abundance ratio, and the ratio of visual extinction to gas column density. Since the extinction at 2.1 μm is one tenth of the visual extinction, the above measurements are consistent with the interpretation that increased extinction at more positive velocities causes the asymmetry of the H_2 profile.

The H_2O masers observed in Orion also have velocities ranging up to $\pm$ 100 km s^{-1}, and the spatial extent of their distribution is very similar to that of the high velocity H_2 and CO emission (Genzel & Downes 1977). Observations, by very long baseline interferometry, of the proper motion of a number of these masers show that they are expanding away from a central region (Genzel *et al.* 1980). These data thus support a picture similar to the one we have adopted to interpret the H_2 data.

The line profiles from the central region do not show a single peak of emission at high velocity, as would be expected from an expanding shell whose back

surface is not seen because of extinction. Instead, they show emission over a continuous range of velocities and, in particular, a maximum of emission at low velocity. It is of interest to determine whether this peak of emission comes from a low velocity part of the flow, which has not expanded very far from the core of the expansion region, or from gas in the molecular cloud surrounding the flow. Calculations have been made to try to reproduce the line profile of the central region, shown in Figure 4, by a model of emission from a sphere of gas of density $n \propto r^{\beta}$, where $\beta \leq 0$ and r is the distance from the center of the sphere. Both the H_2 emission and its absorption by dust were assumed to be directly proportional to the density n. If the gas is expanding at a velocity $V \propto r^{\alpha}$, and α is within a physically realistic range, (*i.e.* $\alpha \leq 1$), the calculations show that, independently of the total amount of extinction, simple spherical expansion models do not reproduce the observed profile of the H_2 emission at low velocities. Two models with $n \propto r^{-2}$ and $V \propto r$, and with respectively 2 and 4 magnitudes of extinction across an optical path passing through the sphere at a projected distance from the center of expansion equal to half the radius of the sphere, are compared, in Figure 7, with the observed average line profile from the central region (Figure 4). The lower extinction model, which gives the best approximation to the H_2 profile for model parameters within the range mentioned above, can reproduce the profile at $V < -20$ km s^{-1} but not at $|V| < 10$ km s^{-1}. For this reason, and from the evidence of increases in intensity at the periphery of the region of H_2 emission (see III.a.*iv*), we conclude that a substantial fraction of the low velocity H_2 emission does not come from the core but from the outside boundary of the expansion region.

b) The Excitation of H_2.

i) Excitation Behind a Shock Front.

Radiative excitation of H_2 and collisional excitation by contact with a heat reservoir have been ruled out both on observational and theoretical grounds (BPN, SRJS, Kwan 1977). The propagation of a shock through a gas cloud provides a constantly renewed supply of excited gas; consequently, many studies have favored models of excitation of H_2 behind a shock front (see *e.g.* Scoville & Kwan 1976, Hollenbach & Shull 1977, Kwan 1977, London *et al.* 1977, BPNB, Chevalier 1980). The calculations have shown that shock fronts moving at velocities from 7 to 24 km s^{-1} with respect to the cloud in which they propagate would heat up the gas behind the shock sufficiently to cause emission from vibrationally excited levels of H_2.

It is a major problem for these models, however, to produce the observed H_2 luminosity. Specifically, the high preshock density which is required may cause the H_2O to dominate the cooling (D. Hollenbach p.c., Hollenbach & McKee 1979, hereafter HM, McKee & Hollenbach 1980), and prevent the column density of gas at $T = 2000$ K from reaching the value observed, $N_{H_2} \approx 3 \times 10^{20}$ cm^{-2} (BNP, SRJS). Because it is critical to the viability of models of excitation behind a shock front, the issue of H_2O cooling is discussed in some detail below.

In order to maintain a specified column density of excited gas, the cooling time τ of the gas must be:

$$\tau \approx \frac{N_{H_2}}{n'_{H_2} V_s} \approx \frac{y N_{H_2}}{n_{H_2} V_s} , \qquad (1)$$

where n'_{H_2} is the preshock density, V_s is the shock velocity, n_{H_2} is the density of the excited gas behind the shock front and y is the ratio of this density to the

preshock density. The value of y is ~ 7 for rotationally and vibrationally excited H_2 gas, in the absence of a strong magnetic field (HM); y can be reduced to a value of ~ 2 if the magnetic field ahead of the shock is as strong as $B_o = 7\,\mu G$, the value estimated by Dyck & Beichman (1974). It is assumed in equation (1) that only a small fraction of the H_2 is dissociated behind the shock. The cooling time can also be expressed as the ratio of the energy in the gas at 2000 K to the cooling rate per unit volume, Λ, at that temperature:

$$\tau \approx \frac{3kT\, n_{H_2}}{\Lambda} \quad , \tag{2}$$

where the value $3kT$ comes from equipartition of the energy between the translational, rotational and vibrational degrees of freedom. Combining (1) and (2), the value of the cooling rate becomes:

$$\Lambda \approx \frac{3kT\, (n_{H_2})^2\, V_s}{y\, N_{H_2}} \quad . \tag{3}$$

It is a good approximation to assume that the cooling of the gas at $T = 2000$ K is due only to H_2, because of its large abundance, and to H_2O, because of its large dipole moment (HM). If the column density N_{H_2} is to be maintained, the sum of the cooling rates of these two molecules must be less than the value given by equation (3).

Equation (3) can be used to obtain a lower limit to the density n_{H_2}. Since H_2 has a low radiation probability, collisions maintain the population of its excited levels in Boltzmann distribution for gas densities above 10^6 cm^{-3} (Kwan 1977), and the H_2 cooling rate is proportional to n_{H_2} (Osterbrock 1974):

$$\Lambda_{H_2} = n_{H_2} \sum_{u,l} f(u)\, A_{ul}\, E_{ul} \, , \tag{4}$$

where $f(u)$ is the fraction of H_2 molecules in upper state u, A_{ul} is the Einstein

coefficient for spontaneous transition between states u and l, and E_{ul} is the energy of the transition. Then equations (3) and (4) give:

$$n_{H_2} \gtrsim \frac{y\, N_{H_2} \sum_{u,l} f(u)\, A_{ul}\, E_{ul}}{3kT\, V_s} \quad . \tag{5}$$

This expression can be evaluated for a shock velocity $V_s = 10\,\mathrm{km\ s^{-1}}$, a compression factor $y = 7$ and a temperature $T = 2000\,\mathrm{K}$, using the values of A_{ul} given by Turner *et al.* (1977), and the values of E_{ul} obtained from Fink *et al.* (1965):

$$n_{H_2} \gtrsim 2 \times 10^8\ \mathrm{cm^{-3}} \quad . \tag{6}$$

Equation (3) also provides an upper limit to x_{H_2O}, the abundance of H_2O relative to H_2. Because of its large radiative deexcitation rate, the cooling rate of H_2O will in general be proportional to the collision rate between H_2 and H_2O. The cooling rate of H_2O can be expressed as

$$\Lambda_{H_2O} = x_{H_2O}\, (n_{H_2})^2\, \sigma \bar{v} \bar{E} \quad , \tag{7}$$

where $\bar{v}$ is the average velocity, $\bar{E}$ is the average energy transfer per collision, and σ is the cross-section. It is assumed in this discussion that the emission from H_2O at 2000 K is optically thin. From (3) and (7) the upper limit on x_{H_2O} is:

$$x_{H_2O} \lesssim \frac{3kT\, V_s}{y\, N_{H_2} \sigma \bar{v} \bar{E}} \quad , \tag{8}$$

It is possible to evaluate $\sigma \bar{v} \bar{E}$ from the calculations of Green (1980) and with the assumptions that all collisional transitions are from the ground state, that the vibrational transitions have much smaller cross-sections than the rotational transitions (HM), and that the value of σ is the same at 2000 K as at 500 K. For a shock velocity $V_s = 10\,\mathrm{km\ s^{-1}}$, a compression factor $y = 7$ and a temperature $T = 2000\,\mathrm{K}$, the limiting value of x_{H_2O} is:

$$x_{H_2O} \lesssim 10^{-6} \quad . \tag{9}$$

Waters *et al.* (1980) have evaluated the abundance of H_2O relative to H_2, in Orion, to be $5 \times 10^{-7} \lesssim x_{H_2O} \lesssim 5 \times 10^{-6}$. Phillips *et al.* (1978) give $n_{H_2O} \approx 8\ cm^{-3}$, This is inconsistent with the values given by Waters *et al.* and the value of n_{H_2} obtained in equation (6).

The values of Waters *et al.* and Phillips *et al.* are probably representative of the abundance of H_2O in the cold gas, and it is necessary to evaluate a possible increase in the abundance of H_2O behind the shock. Since oxygen has the highest cosmic abundance after hydrogen and helium (Cameron 1973), there is a large amount of atomic or molecular oxygen available to form H_2O; the total abundance of the other elements (Cameron) is not sufficient to absorb oxygen entirely in other molecules. From the reaction rates given by Elitzur (1979) it is straightforward to calculate that, at a temperature near 2000 K and a density $n_{H_2} \approx 2 \times 10^8\ cm^{-3}$, the abundance of H relative to H_2 must be kept below a value of $\sim 3 \times 10^{-6}$ in order not to produce so much H_2O in the gas at $T \approx 2000$ K that the cooling time is reduced below the value given in (1).

Even in the most favorable case where all the hydrogen and oxygen is in molecular form ahead of the shock front, this requirement places a very strong constraint on the dissociation rate of H_2 and hence on the velocity of the shock. The dissociation rate of H_2 given by equation (5) of Kwan (1977), which has been obtained from the measurements of Jacobs *et al.* (1967), implies that the postshock temperature cannot reach a value much higher than the observed $T = 2000$ K. The temperature immediately behind the shock front can be related to the shock velocity (HM), and the requirement on this velocity, taking into account the uncertainties in the above calculations, is $7\ km\ s^{-1} \lesssim V_s \lesssim 10\ km\ s^{-1}$.

These restrictions on the shock velocity and on the preshock abundance of H with respect to H_2 can be alleviated if a strong magnetic field lowers the value of y or if the oxygen bearing molecules are depleted by condensation onto grains; even if there is such a depletion in the preshock gas, however, the shock velocity must remain much smaller than $\sim 50\,\mathrm{km\ s^{-1}}$ to avoid evaporation of the molecules frozen on the grains (HM).

The H_2O emission has been assumed, in this discussion, to be optically thin. For a postshock density $n_{H_2} = 2 \times 10^8\ \mathrm{cm^{-3}}$ and a column density of hot gas $N_{H_2} = 3 \times 10^{20}\ \mathrm{cm^{-2}}$, HM show that H_2O emission will become optically thick for a relative abundance $x_{H_2O} \approx 6 \times 10^{-5}$. At such a value of x_{H_2O}, H_2O would dominate the cooling so much that it would be necessary to increase the preshock density to $n'_{H_2} \approx 3 \times 10^8\ \mathrm{cm^{-3}}$, in order to obtain the measured value of N_{H_2}. This value of n'_{H_2} is much higher than estimates of the density of H_2 in the molecular cloud and in the flow at the large distance from the center where H_2 is observed to radiate. The conclusions based on the hypothesis that H_2O emission is optically thin are therefore probably valid. The small range of conditions for which the models of excitation behind a shock front can reproduce the experimental data reduces severely the probability that this is the main mechanism responsible for the excitation of H_2.

ii) Magnetic Precursor Excitation.

Mullan (1971) and Draine (1980) have shown that when the gas ahead of a shock front has a low level of ionization, and when the magnetic field in this gas is reasonably strong, part of the momentum and energy transfer from the gas behind the shock to the gas ahead of the shock is mediated by the magnetic field. The thickness of the shock, in this case, is of the order of the length

required to transfer the momentum contained in the magnetic field to the bulk of the gas by collisions of the charged particles, frozen in the field, with the neutral particles, and this length is large compared to the cooling length. It is therefore possible, in principle, to transform kinetic energy into thermal energy, at a rate large enough to account for the observed column density, without having a very high particle density, since the interaction of the charged particles with the neutral particles can happen over a long distance. The temperature need also not be raised to a very high value, since the time during which a given volume of gas is heated can be large compared to the cooling time.

Draine (p.c.) has calculated that a shock moving at a velocity $V_s = 50\,\mathrm{km\ s^{-1}}$ into a gas cloud of density $n_{H_2} = 1 \times 10^6 \mathrm{cm^{-3}}$, an abundance of ions and electrons $n_i/n_{H_2} = n_e/n_{H_2} = 10^{-7}$, and a magnetic field $B_0 = 5\,\mathrm{mG}$, would have a magnetic precursor with a characteristic length $L \approx 2 \times 10^{15}\,\mathrm{cm}$, where

$$L \propto \frac{B_0^2}{\rho_i \rho_n} \quad , \tag{10}$$

and ρ_i and ρ_n are the mass densities of the charged and neutral particles, respectively. The neutral gas would be heated to $T \approx 2000\,\mathrm{K}$ and the flux emitted by the precursor would be $F \approx 20\,\mathrm{ergs\,cm^{-2}\ s^{-1}}$, sufficient to account for the measured H_2 luminosity. In addition, the neutral gas is accelerated on the average to a velocity of $\sim 5\,\mathrm{km\ s^{-1}}$ and therefore the density increases only by $\sim 10\%$ in the precursor. Since the density does not become very high, cooling by H_2O should be negligible.

A potential problem with this model is the density of ionized particles ahead of the shock. The value assumed above is that which is expected from ionization by cosmic rays only, and it does not take into account ionization by the radiation emitted behind the $50\,\mathrm{km\ s^{-1}}$ shock. Such a shock could generate enough

ultraviolet radiation to ionize a large fraction of the gas before it went through the shock (Shull & McKee 1979). An increase of the ion density would, according to (10), reduce the length of the precursor and hence the column density of gas at $T = 2000$ K. Detailed calculations of the cooling process are needed to determine the interaction between the UV and magnetic precursors.

c) Velocity Range of the Emission.

An important result of the present observations is the fact that the excited gas has a large range of velocities (Figures 4 and 5). On the other hand, the existing models of H_2 excitation do not provide a large acceleration of the excited gas: according to the postshock excitation model, the H_2 emission can be explained only by shocks with velocities below 10 km s^{-1}, and, according to the magnetic precursor model, the H_2 emitting gas is accelerated only to ~ 5 km s^{-1}. This implies that the high velocity emission comes from gas in the flow, and this flow must have a density greater than 10^5 cm^{-3}, at a distance from the center on the order of 10^{17} cm, since the excitation models require densities greater than or equal to 10^6 cm^{-3} to account for the emission at all velocities, and the high velocity emission is seen over an area of $\sim 2.5 \times 10^{17}$ cm in diameter. Two masses of gas colliding with each other at supersonic velocities will have a shock wave moving into each of them; gas in a flow will therefore be excited following a collision of the flow with gas at rest or flowing at lower velocity (Chevalier 1980). On the other hand, as shown in IV.a, simple models of emission from an expanding sphere of excited gas do not reproduce the observed line profiles at low velocity. This suggests that at least part of the low velocity emission comes from gas in the molecular cloud surrounding the expansion region, that is excited by the collision of the flow.

If both the flow and the molecular cloud are spherically symmetric, the profile of the emission line, according to this model, should show a peak of emission at low velocity and a peak of emission at high velocity, rather than emission over a broad range of velocities, such as is seen in Figures 4 and 5. These observed profiles can be explained by emission throughout the expanding sphere from non-uniform flows, where the faster moving gas drifts through the slower moving gas and causes turbulence, or by multiple concentric expanding shells colliding with each other. One of the simplest hypotheses, however, is probably to assume that the gas within the flow has been accelerated to various velocities and interacts with the molecular cloud at different distances from the center, because of density inhomogeneities in the cloud.

The observed spectra of H_2 provide some evidence of such inhomogeneities. The flow appears to have expanded much farther into the molecular cloud to the north and northeast than in the other directions, possibly because it has encountered in that direction a region of lower density. Some gas can be seen moving away from the observer, suggesting that there is less extinction through the flow in that direction. Some gas can also be seen at higher negative velocity than in the central part possibly because gas moving at this velocity has already reached the molecular cloud everywhere but to the north, where it has to travel farther.

Individual spectra in the central region often have profiles which differ significantly from each other. An example of this can be seen by comparing, in Figure 1, the spectra at (47.2,−24 14) and (46.7,−24 17) to those in the south of the central region. The peculiar spectrum at (46.6,−24 21) is characterized by a dip in the integrated intensity at that position (*cf.* BPNB) and by the lack of a well defined peak at low velocity; both features can be explained by a relative

lack, in that direction, of high density cloud material emitting at low velocity. The spectra near Pk 5, in Figure 2, have a distinct shoulder at negative velocity, which seems to imply that a cloud of gas is moving there with a radial velocity of $\sim -50\,\mathrm{km\ s^{-1}}$.

The rapid decrease of the peak intensity of H_2 emission to the east and to the southwest may be due to an increase in the extinction in front of the emission region rather than lower emission in the excited region. The outer contours of the 13" map of BPNB (see Figure 1) are bordered to the east and to the south by the contours of two dense H_2CO clouds (T.L. Wilson, p.c.).

d) Comparison with Other Data.

The line profiles of H_2 and CO extend to similar negative velocities and this similarity has been used in IV.a to argue that both gases had been accelerated to high velocities by the same process. The profiles are not completely similar, however. The line profile of the $J=2\rightarrow 1$ line of CO (Knapp *et al.* 1980) has been superposed on the spectrum of the central region in Figure 4. Even with the large uncertainty in the position of the CO measurement, both profiles probably sample similar areas. The result of the comparison of the two profiles is that the ratio of H_2 to CO emission increases strongly toward negative velocities. Furthermore, the velocity centroid of the $J=2\rightarrow 1$ line of CO shows a change of $4\,\mathrm{km\ s^{-1}}$ along an axis going from the southeast to the northwest of the H_2 emission region (Knapp *et al.* 1980). The H_2 data from the corresponding positions (III.a.ii), however, show no difference in velocity to a 95% level of confidence. This discrepancy may be due to the different methods used in determining the velocity centroid; in the case of CO, the centroid was obtained from the high velocity part of the profiles, while in the case of H_2, the centroid is obtained

from the low velocity part of essentially narrow profiles.

The CO and H_2 emission also differ in their spatial extent. They appear to be centered at the same position but, according to Knapp *et al.*, the CO source size is essentially that of the inner boundary of the H_2 emission. Phillips *et al.* (1977) also have measured a smaller size for emission in the $J=3\rightarrow 2$ transition of CO than the extent of the H_2 emission.

The H_2 emission at $2\,\mu m$ is seen only from gas at $T \geq 1000\,K$ so that a strong heating mechanism is needed. Collisions between clouds offer a natural setting for such mechanisms, and we have proposed that the H_2 emission is coming from the interaction between the flow and the cloud at the boundary of the expansion region. On the other hand, a high temperature is not required to produce CO emission at millimeter wavelengths, and the measured temperature of the high velocity CO is $\sim 100\,K$ (Phillips *et al.* 1977). A simple explanation of the differences between the CO and H_2 data is that CO emission comes from the entire volume of the expansion region rather than mostly from its boundary. For example, the inner part of the expansion region may contribute substantially to the low velocity CO emission. Models of the CO emission from a sphere of gas expanding with a velocity proportional to the distance from the center of expansion have been proposed by Scoville (1980) and Knapp *et al.*.

To explain the observed motion of the H_2O masers, Genzel *et al.* (1980) have proposed a model in which two flows of gas are expanding more or less from the same center, one having a velocity of $\sim 18\,km\,s^{-1}$ independently of distance from the center, and the other having velocities up to $\sim 100\,km\,s^{-1}$. The high velocity masers seem to be distributed preferentially along the boundary between the central and peripheral regions of H_2 emission. If this observation is real, it could be either because the high velocity gas ($V \gtrsim 50\,km\,s^{-1}$) is concentrated

there, or because the collision of the flow with the molecular cloud provides conditions favorable to the inversion of the population of the masing levels. The low velocity masers are concentrated near the infrared cluster.

On the other hand, the H_2 observations do not show any evidence of an increase in intensity or of a large change in the line profile, at the position of the infrared cluster. The observed H_2 profiles do not show a peak of emission near 18 km s^{-1} that would correspond to the flow of the low velocity H_2O masers. This suggests that the region of H_2 emission is distinct from the volume occupied by the infrared continuum sources, in accord with our model. For this reason it may not be possible to use the H_2 data to identify the source of the flow with one of the infrared sources. The positions of the sources are plotted on the maps of Figure 3. The maps show that, among the brighter sources (Downes *et al.* 1980), IRc1 is the closest to the center of the region of high velocity H_2 emission, and both IRc2 and IRc4 are noticeably offset from this center. This may not be significant, however, if, as argued in the previous section, the extent of the emission region is determined in a large part by density inhomogeneities, which, for example, may have let the gas expand farther to the north than to the south. This restriction may apply to other data as well. The CO measurements of Phillips *et al.* (1977) and Knapp *et al.* show some evidence that the high velocity gas extends to the north, as do the distributions of the CH_3OH masers (Matsakis *et al.* 1980) and the high velocity H_2O masers (Genzel & Downes 1977).

The infrared source IRc9 is spatially associated with the northern extent of the high velocity emission. It is unique by its distance away from the rest of the cluster, and it also has a higher color temperature in the near infrared than the other sources (Hilgeman 1970, Wynn-Williams & Becklin 1974). One model which

could explain these characteristics is that sometime during its evolution, IRc9 has created a low density region around itself and that this is the region into which the flow has expanded. If the source is obscured by material at a large distance from it, the reemission at lower temperature from this material will be spatially diluted and will not appear in the spectrum of the source as it does in the case of IRc1. Another possibility is that IRc9 is one of the sources of the flow; even though the assumption has been made throughout the discussion that there was only one source of expanding gas, there is no physical restriction on the number of such sources. A distinct shoulder at a velocity of ~ -50 km s^{-1} in the spectra measured in a 10" region near the position of IRc9 could be explained by such a model. The geometry of the source of H_2 emission implies, however, that IRc9 cannot be the main contributor to the flow. Finally, it must be pointed out that few measurements of IRc9 have been published and its nature and relationship to the molecular cloud are very uncertain.

Although it may not be possible, on the basis of the H_2 data, to say which of the infrared sources is producing the expanding flow, the fact that a dense flow has been proposed to explain the high velocity H_2 emission supports the suggestion of Downes *et al.* (1980) and Knapp *et al.*, that the source must have a very dense stellar wind.

V. SUMMARY.

This paper has presented observations of the velocity profiles of the $v=1\rightarrow 0\ S(1)$, the $v=1\rightarrow 0\ S(0)$ and the $v=2\rightarrow 1\ S(1)$ emission lines of H_2 in the Orion molecular cloud. The main results of these observations are the following:

1) The region of emission has a more or less circular symmetry, and it can be divided into a central region and a peripheral region. The emission lines in

the central region are emitted with a large range of velocities, but almost exclusively at negative velocities (0 to $-100 km\ s^{-1}$); their peak velocity is $\sim -6 km\ s^{-1}$. The emission lines at the periphery are symmetric, they have a width of $\sim 22 km\ s^{-1}$ and their peak velocity is at $0 km\ s^{-1}$. In general, the brightness of the peak emission is larger at the periphery than in the central region.

2) There is no evidence for changes in temperature larger than $\sim \pm 500 K$ from 2000 K over the range of velocities observed.

3) No variation of the line profiles has been detected between 1978 November and 1980 February.

The discussion of these results has led to the following model of the H_2 emission:

1) There is gas undergoing radial expansion at velocities up to $\sim 100 km\ s^{-1}$ within a region of $\sim 2.5 \times 10^{17} cm$ in diameter around the cluster of infrared sources. A major part of the H_2 emission comes from the outside boundary of this expansion region, where the flow collides with the gas in the molecular cloud.

2) The gas is probably excited by shock waves, but the exact mechanism is not understood. Models of excitation behind the shock front are hampered by the fact that H_2O is likely to dominate the cooling at the high density required to account for the H_2 luminosity.

3) It is reasonable to assume that the gas is already moving at velocities close to those observed before it gets excited. It is concluded that the low velocity emission comes from gas in the molecular cloud surrounding the expansion region, while the high velocity emission comes from gas in the

flow.

4) Specific details of the observed spectra suggest the existence of density inhomogeneities within both the flow and the molecular cloud. The role of such inhomogeneities may be important in explaining the observed velocity range of the H_2 emission.

5) While the H_2 emission probably comes mostly from the boundary of the expansion region, CO emission seems to come from the whole volume of the region. The relation of the high velocity H_2O masers to the region of H_2 emission is uncertain because of the lack of understanding of their excitation mechanism in Orion. It appears that the volume occupied by the infrared continuum sources is distinct from that where the H_2 is emitting.

We are grateful to G. Berriman, K. Sellgren, J. Carrasco, J. Frazer and Howard Lanning for help with the observations, and to the staffs of the Mount Wilson Observatory and of Palomar Observatory for their efficient cooperation. We acknowledge useful discussions with B. T. Soifer, K. Matthews, M. Allen, S. Beck, E. E. Becklin, B. T. Draine, R. Genzel, P. Goldreich, D. Hollenbach, G. Knapp, J. Lacy, T. G. Phillips, T. L. Wilson and B. Zuckerman. This work was supported by NSF grants AST77-20516 and AST78-16826 and NASA grants NGL 05-002-207 and NGL 05-002-140. During the early part of this work, D. Nadeau was a fellow of the Natural Science and Engineering Research Council of Canada.

REFERENCES

Abraham, Z., Opher, R., and Raffaelli, J.C. 1979, *I.A.U. Circular*, No. 3415.

Beck, S.C., Lacy, J.H., and Geballe, T.R. 1979, *Ap. J. (Letters)*, **234**, L213.

Beckwith, S., Persson, S.E., Neugebauer, G., and Becklin, E.E. (BPNB) 1978, *Ap. J.*, **223**, 464.

Beckwith, S., Persson, S. E., and Neugebauer, G. (BPN) 1979, *Ap. J.*, **227**, 436.

Cameron, A.G.W. 1973, in *Explosive Nucleosynthesis*, ed. Schramm, D.N., and Arnett, W.D. (Austin: U. of Texas Press).

Chevalier, R. A. 1980, *Astrophys. Lett.* 21, 57.

Dalgarno, A., and Roberge, W.G. 1979, *Ap. J. (Letters)*, **233**, L25.

Downes, D., Genzel, R., Becklin, E.E., and Wynn-Williams, C.G. 1980, preprint.

Draine, B. T., Roberge, W., and Dalgarno, A. 1979, *Bull. AAS*, **11**, 689.

Draine, B. T. 1980, *Ap. J.*, **241**, 1021.

Dyck, H.M., and Beichman, C.A. 1974, *Ap. J.*, **194**, 57.

Elitzur, M. 1979, *Ap. J.*, **229**, 560.

Fink, U., Wiggins, T.A., and Rank, D.H. 1965, *J. Molec. Spectrosc.*, **18**, 384.

Gautier, T. N., III, Fink , U., Treffers, R. P., and Larson, H. P. 1976, *Ap. J. (Letters)*, **207**, L129.

Genzel, and Downes, D. 1977, *Astr. Ap.*, **61**, 117.

Genzel, R., Reid, M.J., Moran, J.M., and Downes, D. 1980, preprint.

Hall, D.N.B., Kleinmann, S.G., Ridgway, S.T., and Gillett, F.C. 1978, *Ap. J. (Letters)*, **223**, L47.

Hilgeman, T. 1970, Ph.D. thesis, California Institute of Technology.

Hollenbach, D. J., and McKee, C. F. (HM) 1979, *Ap. J. Suppl.*, **41**, 555.

———. 1980, *Ap. J. (Letters)*, **241**, L47.

Hollenbach, D.J., and Shull, J.M. 1977, *Ap. J.*, **216**, 419.

Iglesias, E.R., and Silk, J. 1978, *Ap. J.*, **226**, 851.

Jacobs, T.A., Giedt, R.R., and Cohen, N. 1967, *J. Chem. Phys.*, **47**, 54.

Knapp, G.R., Phillips, T.G., Huggins, P.J., and Redman, R.O. 1980, preprint.

Kwan, J. 1977, *Ap. J.*, **216**, 713.

Kwan, J., and Scoville, N.Z. 1976, *Ap. J. (Letters)*, **210**, L39.

London, R., McCray, R., and Chu, Shih-I. 1977, *Ap. J.*, **217**, 442.

Matsakis, D.N., Cheung, A.C., Wright, M.C.H., Askne, J.A., Townes, C.H., and Welch, W.J. 1980, *Ap. J.*, **236**, 481.

McKee, C.F., and Hollenbach, D.J. 1980, *Ann. Rev. Astron. Astrophys.*, **18**, 219.

Mullan, D.J. 1971, *M. N. R. A. S.*, **153**, 145.

Nadeau, D., and Geballe, T.R. (Paper I) 1979, *Ap. J. (Letters)*, **230**, L169.

Nadeau, D., Neugebauer, G., and Geballe, T.R. 1980, in *Interstellar Molecules*, I.A.U. Symp. No. 87, ed. B.H. Andrew (Dordrecht: Reidel).

Ogden, P.M., Roesler, F.L., Larson, H.P., Smith, H.A., Reynolds, R.J., and Scherb, F. 1979, *Ap. J. (Letters)*, **233**, L21.

Osterbrock, D.E. 1974, *Astrophysics of Gaseous Nebulae* (San Francisco: Freeman).

Phillips, T.G., Huggins, P.J., Neugebauer, G., and Werner, M.W. 1977, *Ap. J. (Letters)*, **217**, L161.

Phillips, T.G., Scoville, N.Z., Kwan, J., Huggins, P.J., and Wannier, P.G. 1978, *Ap. J. (Letters)*, **222**, L59.

Scoville, N.Z. 1980, in *Interstellar Molecules*, I.A.U. Symp. No. 87, ed. B.H. Andrew (Dordrecht: Reidel).

Scoville, N.Z., Kleinman, S.G., Hall, D.N.B., and Ridgway, S.T. (SKHR) 1981, preprint.

Shull, J.M., and McKee, C.F. 1979, *Ap. J.*, **227**, 131.

Simon, M., Righini-Cohen, G., Joyce, R.R., and Simon, T. (SRJS) 1979, *Ap. J.*

(Letters), **230**, L175.

Spitzer, L. 1978, *Physical Processes in the Interstellar Medium* (New York: Wiley-Interscience).

Turner, J., Kirby-Docken, K., and Dalgarno, A. 1977, *Ap. J. Suppl.*, **35**, 281.

Waters, J.W., Gustincic, J.J., Kakar, R.K., Kuiper, T.B.H., Roscoe, H.K., Swanson, P.N., Rodriguez Kuiper, E.N., Kerr, A.R., and Thaddeus, P. 1980, *Ap. J.*, **235**, 57.

Wynn-Williams, C.G., and Becklin, E.E. 1974, *Pub. A. S. P.*, **86**, 5.

Zuckerman, B., Kuiper, T.B.G., and Kuiper, E.N. Rodriguez 1976, *Ap. J. (Letters)*, **209**, L137.

TABLE 1. Journal of Observations

Epoch	*Telescope*	*Transition Observed*	*Spectral Resolution* km s^{-1}	*Spatial Resolution* "
78 Oct	2.5 m	$v=1\rightarrow 0$ $S(1)$	20	10
79 Feb	2.5 m	$v=1\rightarrow 0$ $S(1)$	20	10
79 Feb	5 m	$v=1\rightarrow 0$ $S(1)$	20	5
		$v=1\rightarrow 0$ $S(1)$	20	10
		$v=1\rightarrow 0$ $S(0)$	40	10
		$v=2\rightarrow 1$ $S(1)$	40	10
79 Oct	2.5 m	$v=1\rightarrow 0$ $S(1)$	20	10
79 Dec	2.5 m	$v=1\rightarrow 0$ $S(1)$	20	10
80 Feb	5 m	$v=1\rightarrow 0$ $S(1)$	20	10
		$v=1\rightarrow 0$ $S(0)$	20	10
		$v=2\rightarrow 1$ $S(1)$	20	10

FIGURE CAPTIONS

FIGURE 1 Map of the spectra of the $v=1\rightarrow 0$ $S(1)$ line of H_2 measured with a 10" spatial resolution and a 20 km s^{-1} spectral resolution. All the observed profiles are plotted from −122 to +66 km s^{-1} and with the same velocity scale which is shown at the bottom right corner. Velocities are given with respect to the velocity of the molecular cloud. The instrumental spectral profile is plotted near the top left corner of the Figure, with the same scale as the observed profiles. The velocity scale has an absolute uncertainty of ± 3 km s^{-1} and the relative uncertainty between spectra is ± 2 km s^{-1}. All the profiles are plotted with the same peak amplitude. The intersection of the vertical line at $V=0$ with the baseline gives the coordinates of the measurement. The size of the beam is indicated as a shaded circle in the top left corner, and the uncertainty in the pointing is typically ± 2". The intensity contours are from the 13" map of BPNB, and the nomenclature Pk1, Pk2, and Pk5 refers to the 5" map of BPNB. The spectra corresponding to the central region are hatched. The filled-in circles near the center of the map indicate the positions of the brightest infrared continuum sources, *i.e.* from north to south: IRc9, 1, 2, 4. The location of Figure 2 is indicated by a dashed rectangle.

FIGURE 2 Map of the spectra of the $v=1\rightarrow 0$ $S(1)$ line of H_2 measured with a 5" spatial resolution and a 20 km s^{-1} spectral resolution. The description of this Figure is the same as that of Fig. 1, except for small differences due to the different areas covered by each map.

FIGURE 3 Maps of the fraction of the total energy in the line, emitted in a given

velocity interval. Shading of increasing density is used to indicate that 1 to 5%, 5 to 15%, 15 to 30% or 30 to 50% of the integrated intensity comes from the corresponding velocity interval. The shading scale is shown in the lower right corner of Fig. 3a. The velocity interval is indicated in the top left corner of each Figure. On each map a circle 40" in diameter shows the location of the high velocity CO emission. The infrared continuum sources are indicated by filled-in circles and are identified in Fig. 3a.

FIGURE 4 The average intrinsic line profile in the central part of the central region. This profile was obtained by normalizing to a uniform peak amplitude the line profiles in Fig. 1 that were observed in the central region south of −5° 24' 10", by adding them together, and by removing empirically the effect of the instrumental profile. The uncertainty in the velocity of the peak is ± 3 km s^{-1}, but the uncertainty in the velocity of other features of the profile is ± 5 km s^{-1}. The level of the baseline was assumed to be constant across the spectrum. A segment of the line profile of the *J2 line of CO, measured by Knapp *aL. (1980), is shown for comparison. The observations have shown that the CO emission extends in fact to ± 95 km s^{-1}. Because the CO profile is contaminated by emission from the whole molecular cloud at $|V| < 10$ km s^{-1}, it has been scaled so as to have the same amplitude as the H_2 profile at $V = 15$ km s^{-1}.

FIGURE 5 The average intrinsic profile in the northern part of the central region. This profile was obtained by adding, with a weight proportional to the strength of the total signal received, the line profiles in Fig. 1 and Fig. 2 that were observed in the central region north of −5°

24' 12", and by removing empirically the effect of the instrumental profile. The uncertainties in the spectrum are the same as those stated in the caption of Fig. 4. As in Fig. 4 the value of the baseline was assumed to be constant across the region of emission.

FIGURE 6 Comparison of profiles of the $v=1\rightarrow 0\ S(0)$ line (top) with profiles of the $v=2\rightarrow 1\ S(1)$ line (bottom). The coordinates of the observations are indicated in the top right corner of each quadrant. All the spectra have been scaled to the same peak amplitude. The spectra in the left quadrants were measured in identical conditions in 1979 Feb and the velocity scale is the same for both spectra. The spectral resolution of the instrument was $\sim 40\,\mathrm{km\ s^{-1}}$, and the profiles have been smoothed over a $35\,\mathrm{km\ s^{-1}}$ velocity interval. The spectra in the right quadrants were observed in 1980 Feb, with a spectral resolution of $20\,\mathrm{km\ s^{-1}}$. They were also measured in identical conditions, and their velocity scales are the same; no smoothing of these data was done.

FIGURE 7 Two profiles calculated from models of an expanding sphere are shown superposed on the line profile observed in the central region (*cf.* Fig. 4). In both models, $V \propto r$ and $n \propto r^{-2}$, where r is the distance from the center of expansion. The emission and the extinction are assumed proportional to the density n; $V_{max}=80\,\mathrm{km\ s^{-1}}$ and $r_{max}=2\times 10^{17}\,\mathrm{cm}$ (28"). The profiles have been calculated for a distance from the center of expansion equal to the estimate of the average distance of the observed profile from this center. Each calculated profile is normalized to the amplitude of the observed profile at the velocity of the peak of the calculated profile. The extinction quoted is the total extinction through the sphere at a projected dis-

tance midway between the center and r_{max}. See text.

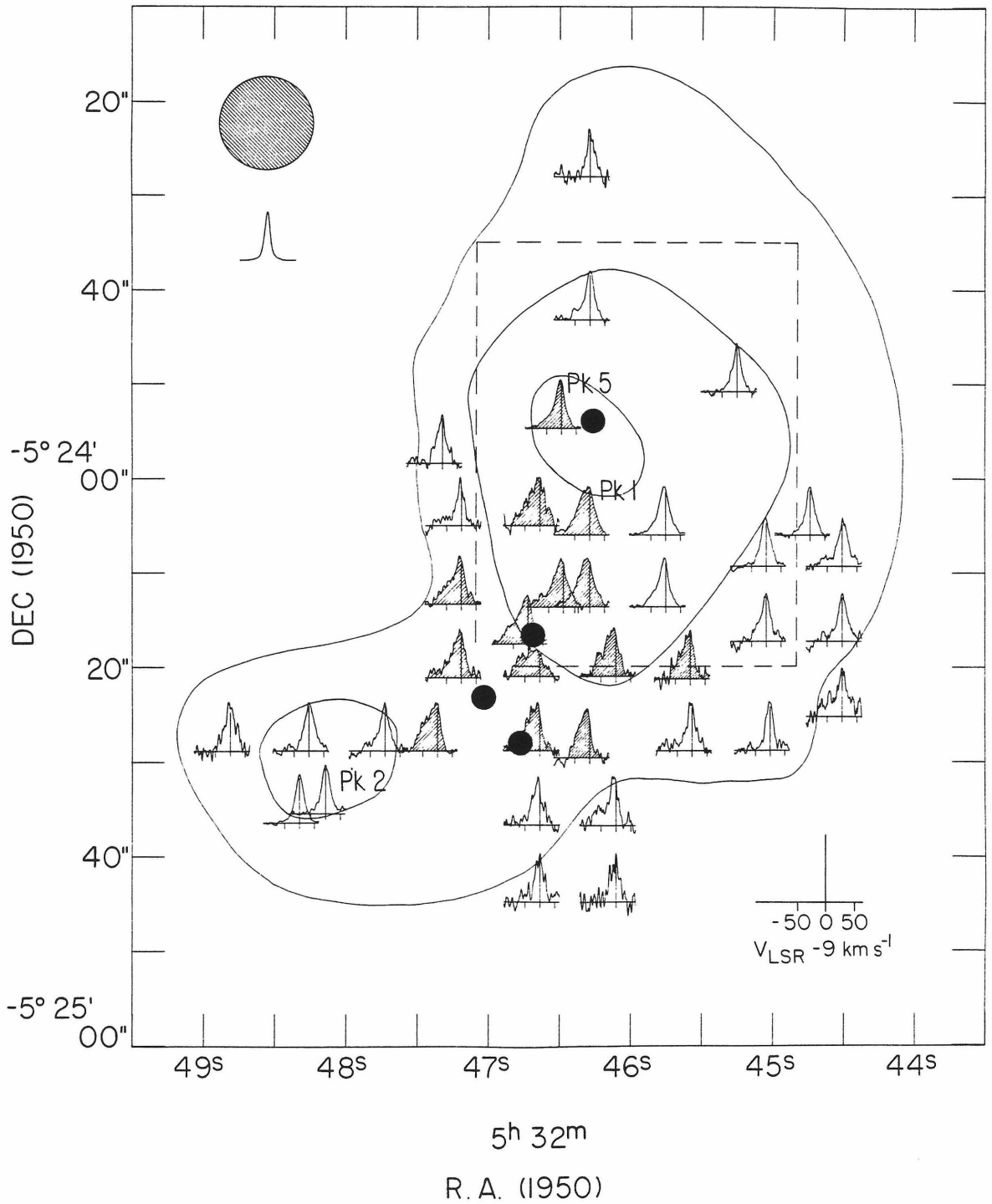
20"
40"
-5° 24'
00"
20"
40"
-5° 25'
00"
DEC (1950)
Pk 5
Pk 1
Pk 2
-50 0 50
V_{LSR} -9 km s^{-1}
49^s
48^s
47^s
46^s
45^s
44^s
5^h 32^m
R. A. (1950)

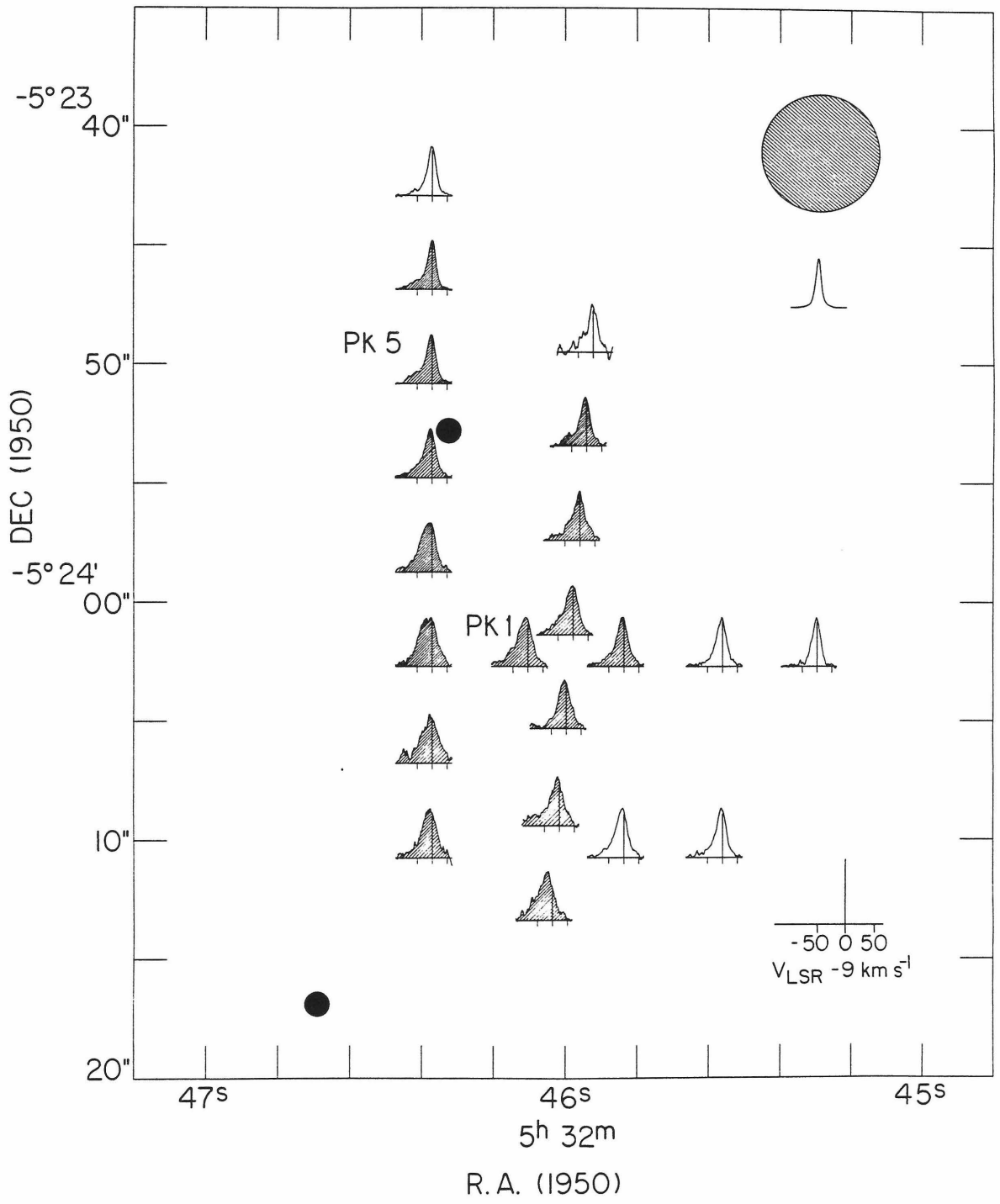
-5° 23
40"
50"
-5° 24'
00"
10"
20"
DEC (1950)
Pk 5
Pk 1
-50 0 50
V_LSR -9 km s^-1
47s
46s
45s
5h 32m
R. A. (1950)

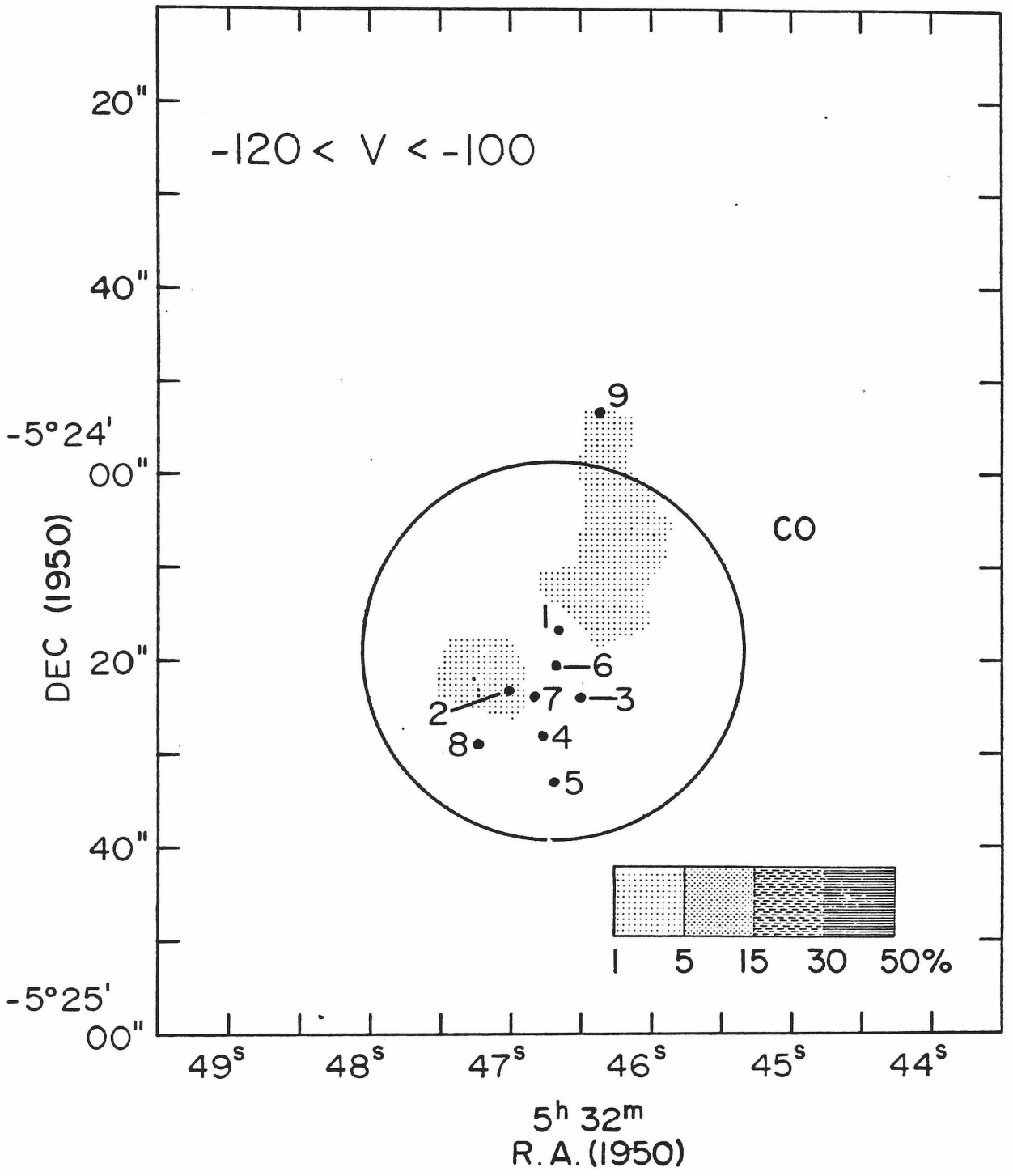
-120 < V < -100
20"
40"
-5°24'
00"
20"
40"
-5°25'
00"
DEC (1950)
CO
9
1
6
2
7
3
8
4
5
1 5 15 30 50%
49s
48s
47s
46s
45s
44s
5h 32m
R.A. (1950)

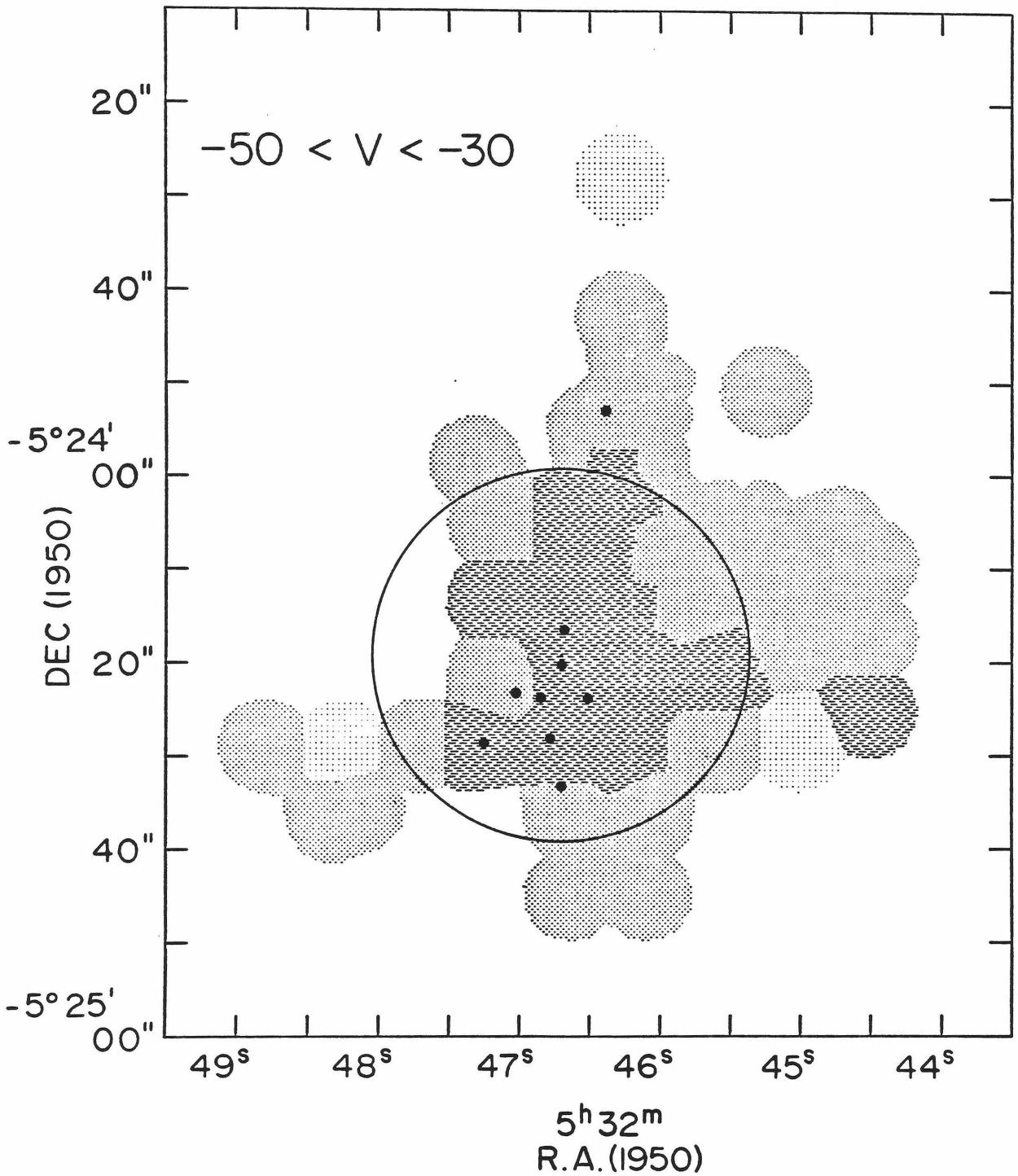
−50 < V < −30
20"
40"
-5°24'
00"
20"
40"
-5°25'
00"
DEC (1950)
49s
48s
47s
46s
45s
44s
5h32m
R.A.(1950)

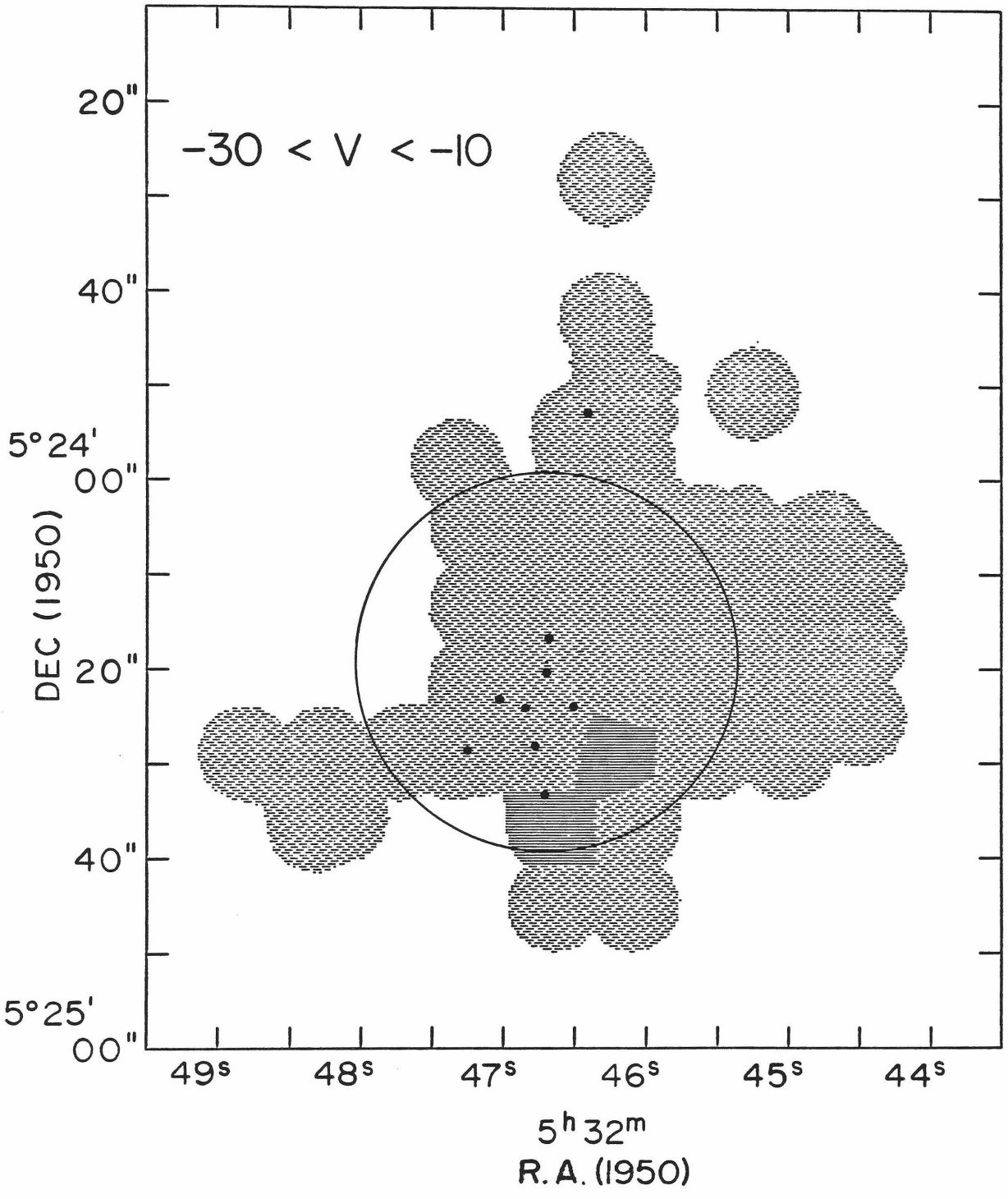
-30 < V < -10
20"
40"
5°24'
00"
20"
40"
5°25'
00"
DEC (1950)
49s
48s
47s
46s
45s
44s
5h 32m
R.A. (1950)

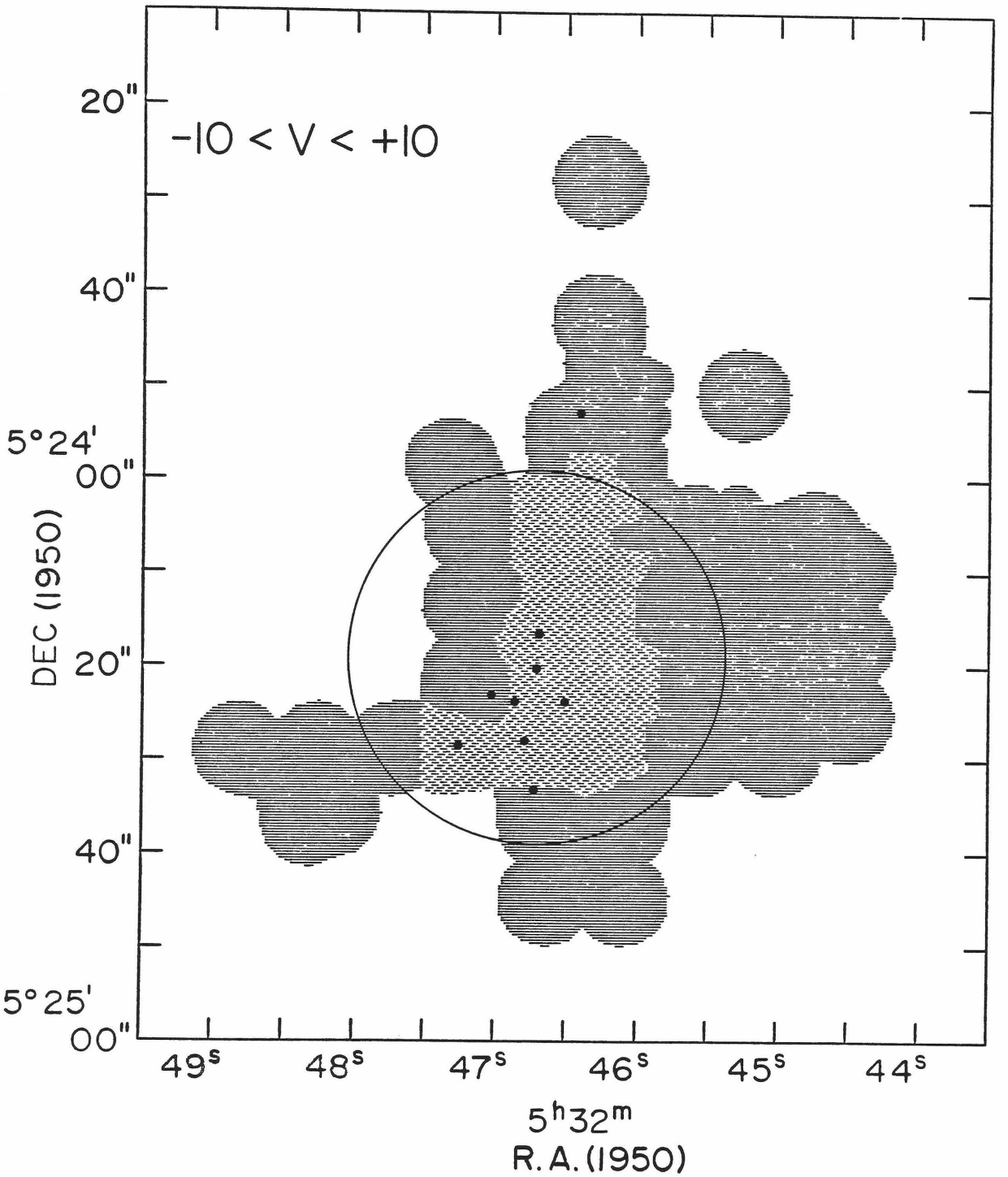
-10 < V < +10
20"
40"
5°24'
00"
20"
40"
5°25'
00"
DEC (1950)
49s
48s
47s
46s
45s
44s
5h32m
R.A. (1950)

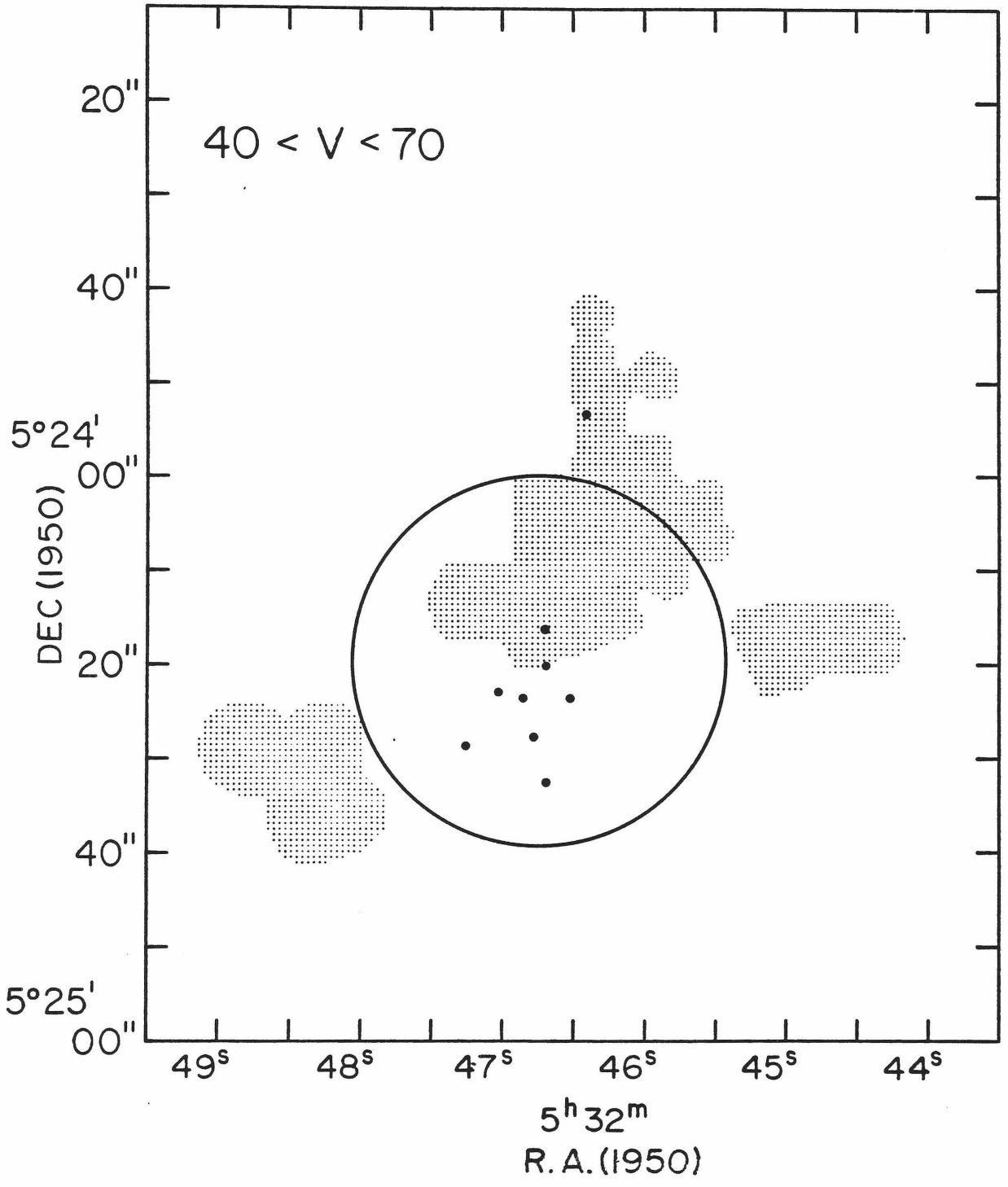
40 < V < 70
20"
40"
5°24'
00"
20"
40"
5°25'
00"
DEC (1950)
49s
48s
47s
46s
45s
44s
5h32m
R.A. (1950)

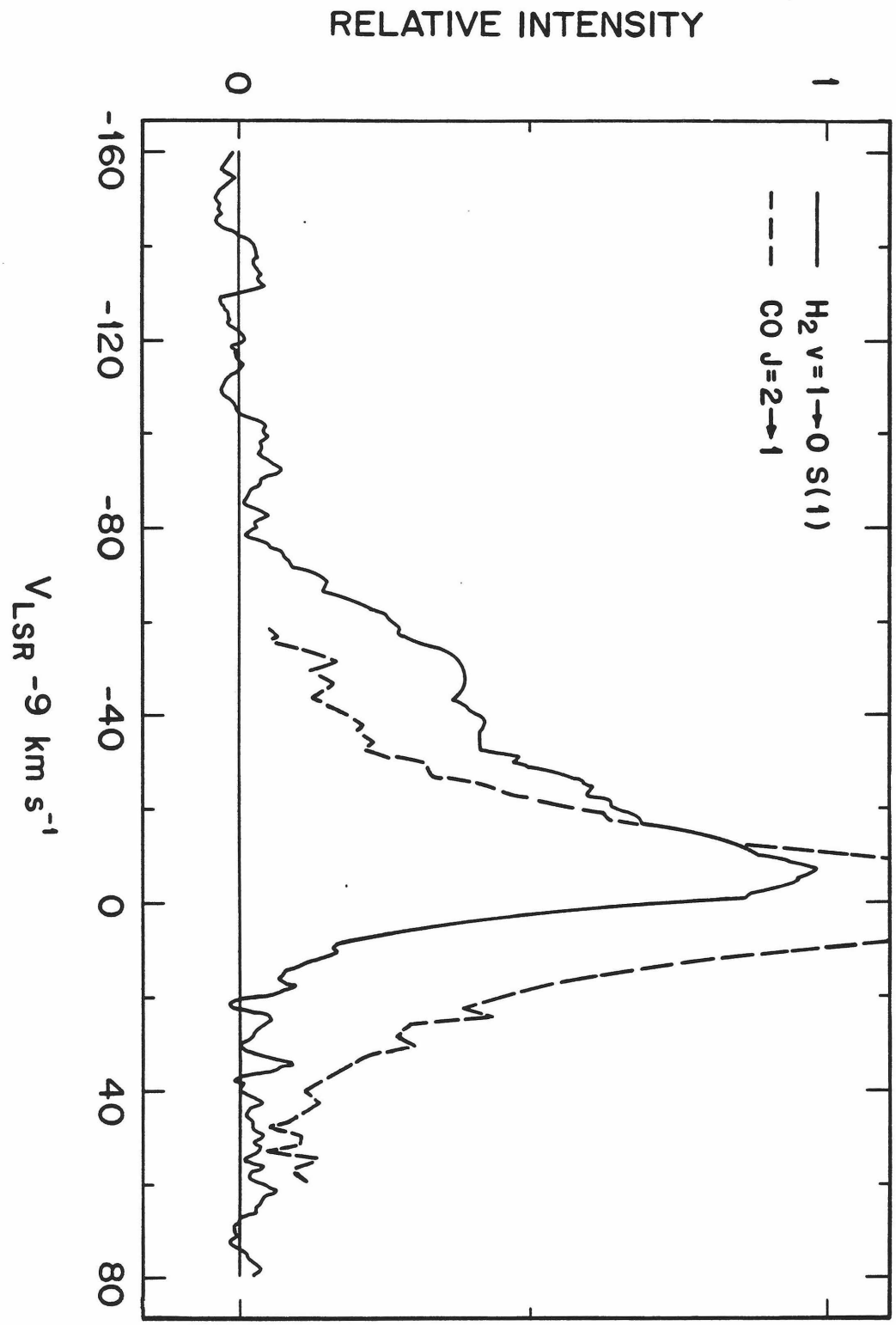
RELATIVE INTENSITY
0
1
H2 v=1→0 S(1)
CO J=2→1
-160
-120
-80
-40
0
40
80
VLSR -9 km s-1

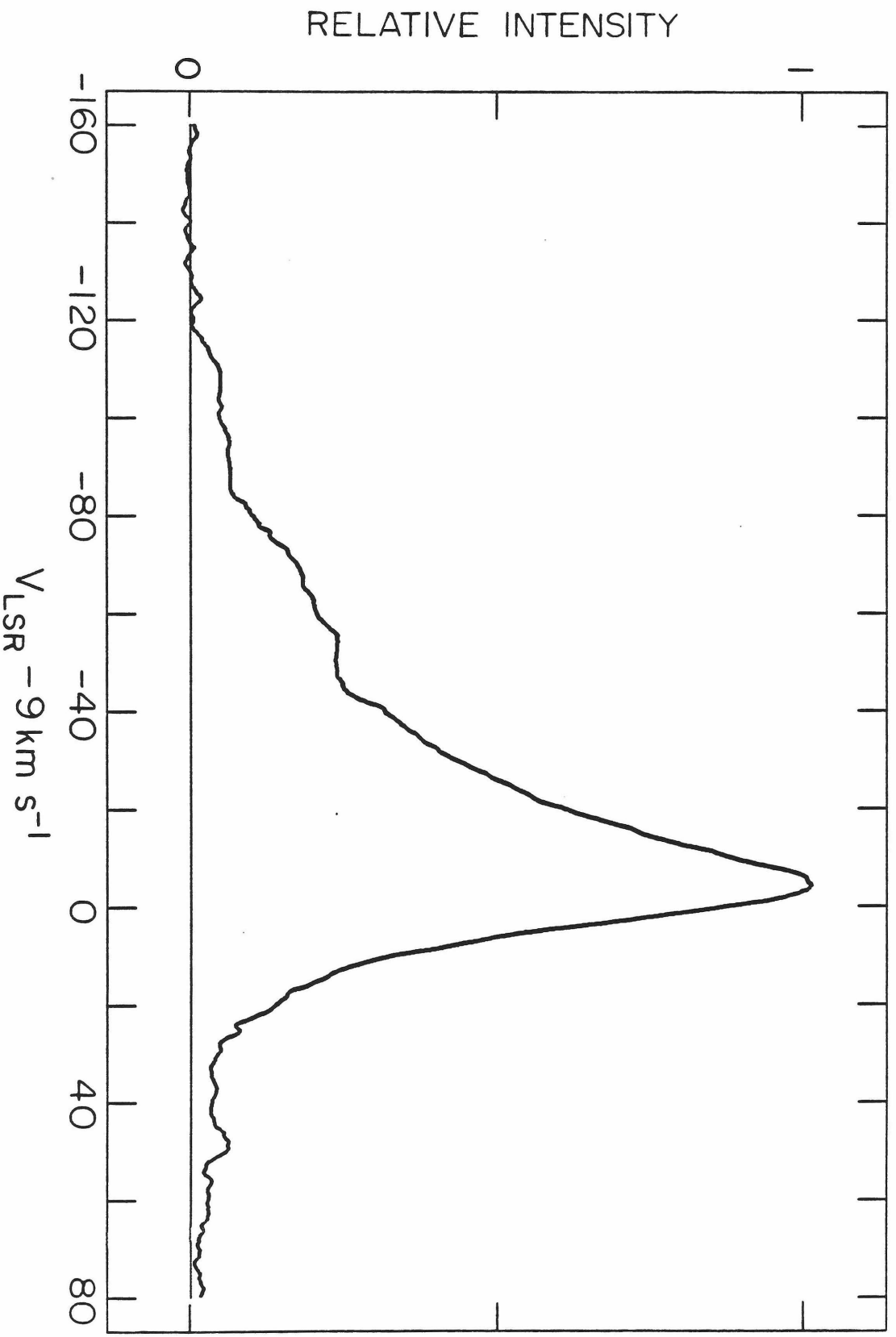
RELATIVE INTENSITY
0
-160
-120
-80
-40
0
40
80
V_{LSR} - 9 km s^{-1}

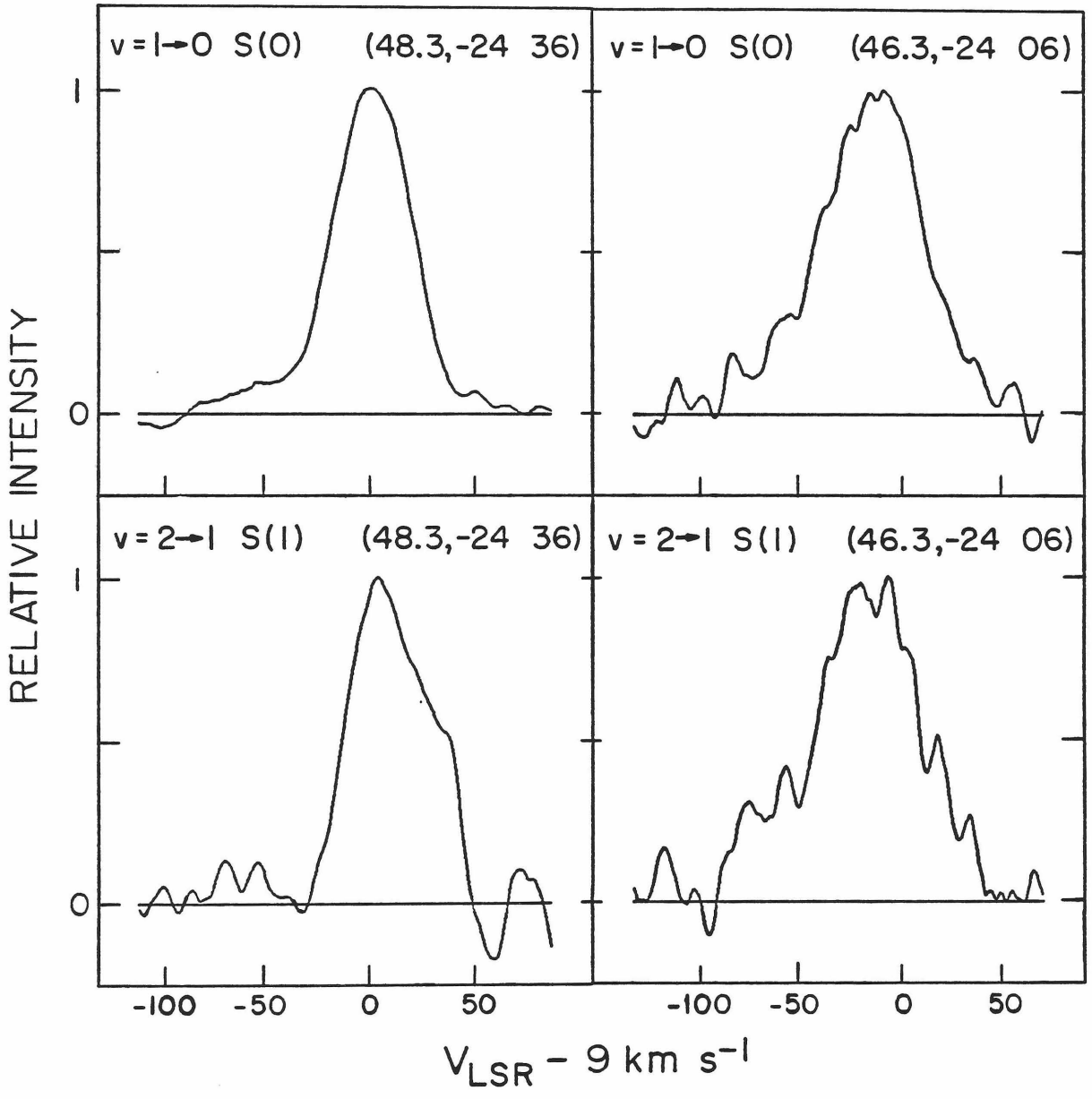
v = 1→0 S(0) (48.3,-24 36)
v = 1→0 S(0) (46.3,-24 06)
v = 2→1 S(1) (48.3,-24 36)
v = 2→1 S(1) (46.3,-24 06)
RELATIVE INTENSITY
1
0
-100
-50
0
50
V_{LSR} - 9 km s^{-1}

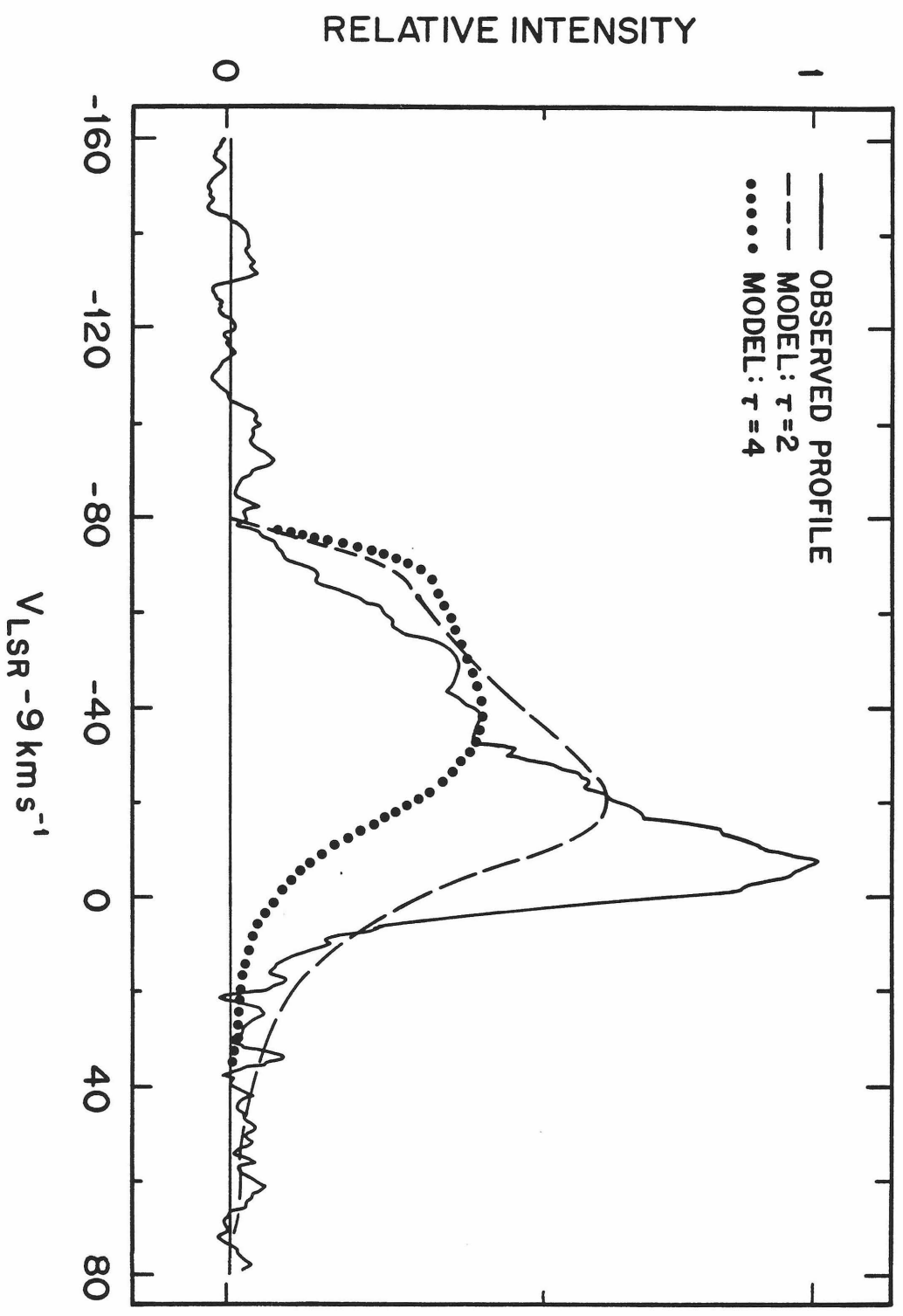
RELATIVE INTENSITY
0
1
OBSERVED PROFILE
MODEL: τ=2
MODEL: τ=4
-160
-120
-80
-40
0
40
80
V_LSR - 9 km s^-1

CONCLUDING REMARKS

In the two previous chapters, a picture of the region of H_2 emission has been developed. There is evidence for a dense flow expanding radially from a point near the infrared continuum sources. The 2μm H_2 emission appears to come mostly from the outside boundary of the expansion region in contrast to the millimeter wave CO emission which appears to come from the entire volume of the flow. The low velocity H_2O masers come from a region near the infrared sources, but the high velocity masers are somewhat concentrated near the boundary of the expansion region. It is hard to identify the source of the expanding gas from the H_2 data but they suggest that IRc9 is associated with a low density region of the molecular cloud. This picture can be used as a framework for further studies of the molecular and continuum sources of emission in the region of the infrared cluster.

Much of the data which have been obtained from the region of expansion still remain puzzling, however. For example a source of NH_3 emission has been observed at low velocity near the source IRc4 (Barrett *aL 1977, Wilson *aL 1979). The CH_3OH masers also have low velocities and are concentrated mainly near the IRc1-IRc4 region (Matsakis *aL 1980). These data could be explained by density inhomogeneities similar to those evidenced by the H_2 data. The advent of millimeter wave interferometers will probably show much structure within the expansion region.

Since the collisions between the flow and the molecular cloud will happen at random there should be a fraction of these collisions for which the difference in velocities between the flow and the cloud will be such that the gas is ionized. This applies to both models of the excitation presented in Paper II, since mag-

netic precursors also are followed by strong shocks. It should then be possible to detect recombination lines in the near-infrared from an area similar to the size of the region where the high velocity gas is observed.

When this research was started, models of excitation behind a shock front had been proposed to explain the temperature and intensity of the H_2 observed at 2 μm. These models required the shock velocity to be between 7 and 24 km s^{-1} in order to excite H_2 without dissociating it completely. The velocity of some of the H_2 gas was subsequently observed to be much higher than the upper limit of 24 km s^{-1}. Chevalier (1980) has suggested that this could be explained within the context of the earlier models if the flow has a high density with respect to the gas it collides with, since a low velocity shock will propagate into the flow and the excited gas will nonetheless be seen at high velocity. Cooling by H_2O, however, causes a more serious problem to models of excitation behind a shock front. Many uncertainties exist in the values used to calculate the cooling rate of H_2O, and the observed column density of H_2 is itself uncertain by a factor of 3. Better values could change the situation either in favor or against the models, unless a satisfactory way is found to keep the densities of H_2 and H_2O behind the shock front to values low enough to limit the cooling by H_2O. Of course, it is always possible that a small fraction of the emission comes from behind the shock front.

The main advantage of the magnetic precursor model is that the gas is kept hot over a large distance ahead of the shock front. The volume density of the gas can therefore be kept to a relatively low value. The calculations which have been made from this model, so far, put stringent requirements on some of the parameters of the region of emission. In particular, the intensity of the magnetic field must be very high and the degree of ionization of the gas must be

very low. It is clear that additional detailed calculations are needed before it is possible to conclude in favor of any model.

One important question that remains unsolved is whether the observed gas flow is a unique event or whether it is recurrent. From the estimates of the column density of gas in front of the region of emission (Hall *aL 1978, Beckwith *aL 1979, Simon *aL 1979), it appears that not more than a few times the mass presently in the flow may have flowed out of the region previously, or the molecular cloud would have disrupted. This means that the events witnessed at the present time have not lasted for more than $\sim 10^{-4}$ years. Since at least a few other sources of H_2 emission in molecular clouds have luminosities similar to that of Orion (Fischer *aL 1980a, b), a short period of intense flow would imply that the processes that lead to such a flow, *e.g.* possibly the formation of a massive star, occur frequently in molecular clouds. Future observations should determine if these sources show the presence of an outflow similar to that observed in Orion.

REFERENCES

Barrett, A.H., Ho, P.T.P., and Myers, P.C. 1977, *Ap. J. (Letters)*, **211**, L39.

Beckwith, S., Persson, S. E., and Neugebauer, G. 1979, *Ap. J.*, **227**, 436.

Chevalier, R. A. 1980, preprint.

Fischer, J., Righini-Cohen, G., and Simon, M. 1980a, *Ap. J. (Letters)*, **238**, L155.

Fischer, J., Righini-Cohen, G., Simon, M., Joyce, R.R., and Simon, T. 1980b, *Ap. J. (Letters)*, **240**, L95.

Hall, D.N.B., Kleinmann, S.G., Ridgway, S.T., and Gillett, F.C. 1978, *Ap. J. (Letters)*, **223**, L47.

Matsakis, D.N., Cheung, A.C., Wright, M.C.H., Askne, J.A., Townes, C.H., and Welch, W.J. 1980, *Ap. J.*, **236**, 481.

Simon, M., Righini-Cohen, G., Joyce, R.R., and Simon, T. 1979, *Ap. J. (Letters)*, **230**, L175.

Wilson, T.L., Downes, D., and Bieging, J. 1979, *Astr. Ap.*, **71**, 275.

APPENDIX

INSTRUMENTATION

I. DESCRIPTION OF THE INSTRUMENT.

All the observations presented in this thesis were made with a single-stage piezoelectrically scanned Fabry-Pérot interferometer coupled to an InSb detector. A cooled variable filter with a resolution $\Delta\lambda/\lambda = 1.3\%$ provided low-resolution filtering. A schematic representation of the instrument and of the data recording apparatus is shown on the following page.

The dewar contains an InSb photovoltaic cell in contact with the surface of a container of solid nitrogen maintained at ~55 K by pumping of the evaporating N_2. A field lens projects an image of the primary mirror on the cell, ensuring a uniform sensitivity over the area of the sky observed. A circular diaphragm (a) in the focal plane can be varied between 0.5 and 4.0 mm, which corresponds to diameters of 2.5" to 20" on the sky for the f/16 bent Cassegrain focus of the 2.5 m telescope on Mt. Wilson, and half of these values for the f/16 Cassegrain focus of the 5 m telescope at Palomar. The upper limit on the size of the beam is set by the design of the beam switching optics (h,i,j). A continuously variable filter wheel with a resolution $\Delta\lambda/\lambda = 1.3\%$, also maintained cold inside the dewar, limits the background light and the number of orders of transmission of the Fabry-Pérot admitted to the detector.

The f/16 beam seen by the detector is produced by a spherical mirror (b) which focuses a collimated beam transmitted by the Fabry-Pérot. The collimated beam is formed by a second spherical mirror (e) which collimates the f/16 beam coming from the telescope. The center of the gap in the Fabry-Pérot

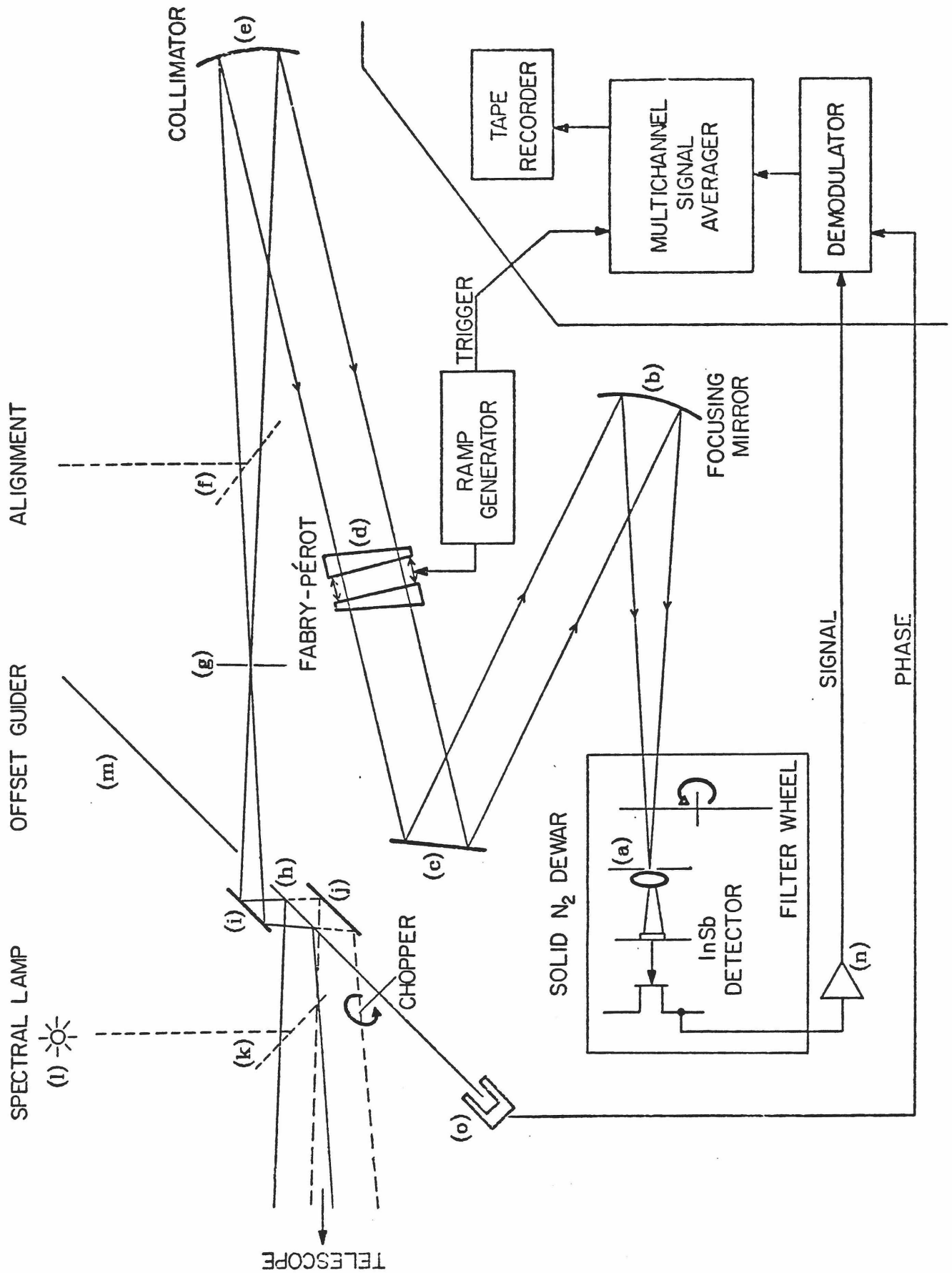
COLLIMATOR
(e)
ALIGNMENT
(f)
OFFSET GUIDER
(g)
FABRY-PÉROT
(d)
(m)
SPECTRAL LAMP
(l)
(k)
(i)
(h)
(j)
CHOPPER
TELESCOPE
(c)
(o)
TRIGGER
RAMP GENERATOR
(b)
FOCUSING MIRROR
SOLID N_2 DEWAR
(a)
InSb DETECTOR
FILTER WHEEL
(n)
SIGNAL
PHASE
TAPE RECORDER
MULTICHANNEL SIGNAL AVERAGER
DEMODULATOR

is at the focus of both spherical mirrors, and an image of the primary is formed at the interferometer. A flat mirror (c) is in the light path between the Fabry-Pérot and the focusing mirror for the sole purpose of orienting the beam in a direction appropriate to enter the dewar. The beam seen by the detector is modulated at a frequency of 10 Hz by alternately switching between two areas of the sky, one of which is on the source and the other a small distance away from the source. The beam switching is done by a rotating chopper wheel (h). An offset guider (m) enables guiding on visible objects, generally to the east of the source, in an area of the sky 8' × 16' (R.A. × DEC.) at the 2.5 m telescope on Mt. Wilson, and half this size at the 5 m telescope at Palomar.

The light from a spectral lamp (l) can be injected into one of the beams (k) to calibrate the interferometer and check the parallelism of its reflecting surfaces. This check is done visually by looking at the light from a mercury vapor lamp (mostly λ5461 Å) reflected by the Fabry-Pérot. For this purpose, a diaphragm (g) is closed in the focal plane to the size of a pinhole and a beam splitter (f) sends the light reflected by the Fabry-Pérot to the observer.

The alignment of the optics is done by having a laser beam oriented perpendicular to the base plate of the instrument and reflected off the chopper wheel (h) and mirror (i) so that it goes through the center of diaphragm (g), which is closed to the size of a pinhole. Starting with mirror (i), each mirror along the optical path is aligned so as to reflect the beam to the center of the next optical component, including the Fabry-Pérot. The mirror (k) is aligned last, by looking at the light of a lamp at (l) from the detector end of the optical path. The reference mirror (j) normally is aligned when the instrument is on the telescope and the relative position of the beams on the sky can be checked.

The scanning of the spectrum is done by varying piezoelectrically the spacing between the two reflecting surfaces of the Fabry-Pérot under the control of a ramp generator. The signal from the infrared detector, after going through a preamplification stage (n) outside the dewar, is sent together with the phase of the chopper (o) to a demodulator (lock-in amplifier), and the rectified signal is fed to a multichannel signal averager where it is digitized. The ramp generator triggers the start of a function of the signal averager by which the digitized signal is integrated during a preset interval of time, and the integrated signal is channeled to successive bins of the memory of the averager. Hence a given channel corresponds to a particular spacing of the interferometer as determined by the calibration. At the end of a measurement, which usually involves many scans of the spectrum, the data are sent to a tape recorder.

The Fabry-Pérot interferometer used in this instrument is a model TL-38IR made by Burleigh, Inc., and the ramp generator is a model RC-42 made by the same company. The dewar used with the instrument is dewar number D-50 of the Caltech infrared astronomy group. The sensitivity of the instrument for the measurement of the line profiles can be expressed in the following way: a change in the measured line profile between two adjacent resolution elements will be detected at the 1σ level in one second of integration if the difference in the intrinsic signal between the two resolution elements is $\sim 3 \times 10^{-7}$ergs s^{-1}.

II. PRINCIPLE OF OPERATION.

The theory of the use of the Fabry-Pérot interferometer for astronomical purposes has been reviewed by Vaughan (1967) and Jacquinot (1960). These reviews form the basis for the following remarks.

The Fabry-Pérot interferometer is a wavelength filter with a transmission described by the Airy function:

$$A(\lambda) = \left(\frac{1-K}{1-R}\right)^2 \times \frac{1}{1+\frac{4R}{(1-R)^2}\sin^2\left(\frac{2\pi l\cos\theta}{\lambda}\right)} \quad , \tag{A.1}$$

where K is the absorptance and R the reflectance of the reflecting surfaces, l is the spacing between the two surfaces, θ is the angle of incidence of the light with respect to the normal to the surfaces, and λ is the wavelength of the transmitted light in the medium between the reflecting surfaces. This medium is air for the instrument described here.

In the ideal case where the reflectance is perfect ($R=1$), the spacing l is constant across the reflecting surfaces, and the angle of incidence θ is unique, the transmission function is a set of Dirac delta functions:

$$A(\lambda) \propto \sum_{m=0}^{\infty} \delta\left(m - \frac{2l\cos\theta}{\lambda}\right) \quad , \tag{A.2}$$

where the integer m is the order of transmission, and the quantity

$$Q = \Delta\left(\frac{1}{\lambda}\right) = \frac{1}{2l\cos\theta} \tag{A.3}$$

is the free spectral range, i.e. the range in reciprocal wavelength between two transmission peaks. In actual cases, none of the above ideal conditions is fulfilled, and the transmission function becomes a convolution of the three functions

$$I(\lambda) = A(\lambda) \otimes D(\lambda) \otimes F(\lambda) \quad , \tag{A.4}$$

where $A(\lambda)$, the Airy function, takes into account the effect of a reflectance $R < 1$, $D(\lambda)$ takes into account the nonuniformity of the spacing across the reflecting surfaces, and $F(\lambda)$ takes into account the range of angles of incidence from a finite aperture.

a) The Reflectance Finesse.

If the reflectance $R < 1$, the value of $A(\lambda)$ (equation A.1) remains finite even when $\lambda = (2l\cos\theta)/m$, and the transmission peaks have a finite full width at half maximum. The ratio of this width to the free spectral range is called the *reflectance finesse* N_R, which can be derived from $A(\lambda)$:

$$N_R = \frac{\pi\sqrt{R}}{1-R} \quad . \tag{A.5}$$

Table A.1 shows the value of the reflectance and of the reflectance finesse as a function of wavelength for the Fabry-Pérot interferometer used in this research project.

b) The Flatness Finesse.

The transmission peaks would have a finite width even for a reflectance $R = 1$ and a single angle of incidence, because of the imperfect flatness and parallelism of the reflecting surfaces. These imperfections are described by the function $D(\lambda)$.

The plates used for this research project are slightly concave and may also have random nonuniformities on a smaller scale. These defects are the limiting factor of the overall finesse of the instrument, which has been found to have a value $N \approx 17$ at a wavelength of 2.12 μm and $N \approx 20$ at 2.25 μm. The deviations from parallelism due to misalignement of the plates are monitored during the observations, and their effect on the finesse is usually very small. Since an image of the primary is formed at the interferometer, all points of the source observed illuminate the same area at the interferometer so that the measurements should be insensitive to variations of the spacing across the surface of the reflecting plates.

TABLE A.1. Reflectance Finesse

Wavelength λ μm	*Reflectance* R	*Reflectance Finesse* N_R
2.00	0.75	11
2.05	0.88	25
2.10	0.918	37
2.15	0.935	47
2.20	0.937	48
2.25	0.935	47
2.30	0.930	43
2.35	0.920	38
2.40	0.908	33
2.45	0.89	27
2.50	0.87	23

c) The Effect of a Finite Diaphragm.

The diaphragm that determines the solid angle observed in the sky also determines the solid angle seen by the interferometer. Even for a reflectance $R=1$ and for perfect flatness and parallelism of the reflecting surfaces, the transmission peaks would have a finite width due to the range of angles of incidence on the interferometer. This width does not depend on the order of interference as did the widths due to a finite reflectance and to nonuniformities. It limits the resolving power to a value less or equal to

$$R_F = \frac{2\pi}{\Omega_F} \quad , \tag{A.8}$$

where

$$\Omega_F = \frac{\pi d^2}{4f^2 d_F^2} \quad , \tag{A.9}$$

and d is the diameter of the diaphragm, f is the focal ratio of the beam seen by the detector and d_F is the diameter of the illuminated area of the Fabry-Pérot plates.

The design of the present instrument uses a circular diaphragm centered on the optical axis of the Fabry-Pérot. The focal ratio is f/16, the diameter of the illuminated area of the plates is 25 mm and the diaphragm can be opened up to 4 mm. These parameters give a linewidth of 2 km s^{-1} for a 20" beam on the sky at the 2.5 m telescope. For the free spectral range of ~ 300 km s^{-1} used normally, the diaphragm finesse $N_F = 150$, and its effect on the overall finesse is negligible.

On the other hand, the use of a finite circular diaphragm also shifts the peak of transmission with respect to purely axial illumination of the Fabry-Pérot. This effect has been noted by Vaughan; our analysis, however, gives a value of the shift that differs from his. As the angle θ is increased from an original value of zero, a decrease in λ must compensate the decrease in $\cos\theta$ in order to stay at a maximum of the Airy function $A(\lambda)$ (*cf.* equation A.1). The shift in wavelength is obtained by finding the wavelength that maximizes the value of the integral of $A(\lambda)$ over the area of the diaphragm. This gives

$$\Delta\lambda = \lambda_{(\theta=0)} \frac{\Omega_F}{4\pi} \quad . \tag{A.10}$$

The shift in wavelength for a change in the size of the diaphragm of the present instrument from a diameter of 1 mm to 6 mm, was measured to be

$$\frac{\Delta\lambda}{\lambda} = -1.18 \pm .1 \times 10^{-5} \quad . \tag{A.11}$$

The value calculated for the same parameters is

$$\frac{\Delta\lambda}{\lambda} = -1.32 \times 10^{-5} \quad . \tag{A.12}$$

The size of the diaphragm used to measure the source is normally the same as that used to measure the calibration line, and the shift in wavelength will be canceled by the calibration. This shift could cause an error of a few km s^{-1} if the source had a size small with respect to the diaphragm used.

III. F-P SPECTROSCOPY FOR FUN AND PROFIT.

This section is no more than a detailed description on how to run the instrument built for this research project. It has been written mainly because this has been the first use of the technique of Fabry-Pérot spectroscopy in the infrared astronomy group at Caltech, and it is intended as a handy reference for those who would want to use the instrument in the future.

a) How it works.

To scan the spectrum, the transmitted wavelength is varied by changing the spacing between the reflecting plates of the interferometer. One of the reflecting plates is kept fixed with respect to the body of the Fabry-Pérot and the other one is moved by three stacks of piezoelectrical crystals, set 120° apart around the circumference of the plate, and on each of which a variable voltage is applied. The voltage used to scan the spectrum has a saw-tooth waveform with a slow increase of its amplitude. The effect of increasing the voltage on the piezoelectric stacks is to decrease the spacing between the plates, so that **the scans are made from longer to shorter wavelengths.**

The sensitivity of the stacks is $\sim 0.005\,\mu m\ V^{-1}$, and the amplitude needed to scan one free spectral range at $2\,\mu m$ is $\sim 200\,V$. The amplitude of the signal from the ramp generator can be varied up to 1000 V, which amounts to 5 free spectral ranges at $2\,\mu m$. The time taken to scan the spectrum can be varied over a large range. It is advantageous to scan quickly to reduce the effect of variations in the transmission of the atmosphere, but limits are imposed by the time constant of the detecting system. In practice, scanning is done generally over 1.25 free spectral range in 20.5 seconds.

b) Alignment of the plates.

For the Fabry-Pérot to perform as an interferometer, its reflecting surfaces must be kept parallel to a high accuracy. The alignment of the plates is done in three steps. A rough mechanical alignment serves to create the interference pattern, by tilting the plate that remains fixed during the scanning so as to superpose the multiple reflections of a narrow laser beam transmitted through the Fabry-Pérot. The plate is held against the body of the interferometer by three screws, two of which have pairs of Belleville spring washers which can be compressed to tilt the plate. A finer mechanical alignment brings the plates in near-perfect alignment. This is done by tightening three set screws against three tongues which are part of the fixed plate holder, thereby flexing the holder and causing a small tilt of the plate. It should be noted that these set screws must be loosened before the rough mechanical alignment is performed. A laser beam that illuminates a good fraction of the plates is required to see the interference pattern.

The last step of the alignment procedure is done by varying independently the voltages on each of the three piezoelectric stacks. Although a perfect align-

ment can be achieved mechanically, the application of a voltage to the piezoelectric stacks generally disturbs the alignment, which must be restored by setting different bias voltages on each of the three stacks. This last step of the alignment is repeated at regular intervals during the period of observations to maintain the parallelism of the plates. While the two steps of mechanical alignment are performed outside of the instrument, the electrical alignment is done with the Fabry-Pérot installed as in Figure 1. In reference to this figure, the light from a mercury lamp at (l) is injected into the light path (k), and the observer sees its reflection off the Fabry-Pérot into the beamsplitter at (f). The diaphragm is usually closed to the size of a pinhole for increased sharpness of the interference pattern, but may left partly open for a greater ease in finding the location of the reflected beam.

The plates are made of quartz, and therefore transparent to visible light. In addition, the reflectance of the dielectric coatings is high enough at the wavelength of the green line of mercury (λ5461Å) that a reasonably sharp interference pattern is formed, and the parallelism of the reflecting surfaces can be estimated visually. This has the advantages of a high sensitivity to misalignment since the wavelength of the mercury line is four times shorter than the observed 2 μm lines, and a high efficiency since the appearance of the pattern shows at once in which direction and by how much the alignment of the plates must be corrected.

The most successful procedure is to start with all three bias voltages set at mid-range. Then, if the Fabry-Pérot has been put into the instrument in a conventional orientation (*e.g.* with the cable coming out of the body of the Fabry-Pérot precisely below the optical axis and toward the collimating mirror), the direction in which each of the three bias voltage knobs affects the alignment

is well defined. To align, it is best to rotate by an angle θ the knob affecting the tilt in the direction of the pattern center and by an angle $-\theta/2$ each of the two other knobs, thereby canceling to first order any shift of the starting point of the scan. This is especially useful when correcting the alignment between two sets of observations.

If the misalignment is severe, the pattern observed will be a set of straight parallel fringes moving toward the imaginary center of the pattern. As this center is brought closer to the observed fringes, the fringes become more distant and curve toward the center. The alignment is optimum when the pattern is a set of rough dark rings vanishing at the center of the image of the reflecting plate. Before the end of the alignment procedure, the amplitude and starting point of the scan should have been set approximately to the right value. A scan during which 5 rings are seen to vanish in the pattern of the green line of mercury covers approximately 1.25 orders of interference at 2.1 μm.

If the vanishing point of the rings is seen to shift across the reflecting plate by a large amount, the ratio of the slopes of the voltage ramps on each of the piezoelectric stacks should be corrected by using the appropriate knobs. This tedious operation needs to be done only occasionally.

The stability of the alignment of the Fabry-Pérot is a major factor of the efficiency of collecting accurate spectral data. To obtain a good stability, it is best to do the mechanical alignment at least 24 hrs before the time of the observations. The fine mechanical alignment should be improved after the interferometer has been left sitting for a period of several hours. It is also important, when doing spectral measurements, to keep the interferometer scanning continuously. Because of capacitive effects in the piezoelectric crystals, the starting point of the scans will drift, immediately after the ramp voltage is

turned on, by an amount decreasing on a time scale of a few minutes. Also because of these capacitive effects the scanning is non-linear; this is discussed in a later section.

c) Measuring the Spectrum.

Most of the measurements presented in this thesis followed the standard procedure which follows. Once the interferometer has been aligned, the scanning amplitude is set to cover 1.25 orders in 20.5 seconds, by adjustment of the knobs controlling the amplitude of the ramp voltage and the bias voltage common to all three piezoelectric stacks, so that the spectral line used for calibration appears, in two successive orders, near channels 940 and 130 of the 1024-channel memory of the multichannel analyzer. The integration time per channel is 20 msec and the time for a complete cycling of the memory is sligthly less than the period of the scan, so that the multichannel analyzer is ready to accept the trigger signal from the ramp generator at the beginning of each new scan. The position of the calibration lines has been chosen so that their profiles are entirely within the scan length, while allowing for drifts during the observations and avoiding the early part of the scan.

The spectral calibration of the scans requires, in addition to the position of the calibration lines, the knowledge of the particular order of interference in which the line is measured and knowledge of the non-linearity of the scan. The procedure to obtain these quantities is outlined below.

d) Choice of the Appropriate Spacing.

The spacing between the plates of the interferometer can be varied by substituting rings of different thicknesses between one of the plate holders and the

body of the interferometer. Stainless steel shims have also been used when a spacer of standard thickness was inappropriate. The use of these shims does not affect the performance of the interferometer.

The principal factor that determines the choice of a particular spacing is the spectral resolution needed for a measurement. The spectral resolution $\lambda/\Delta\lambda$ can be obtained from (A.4) and (A.6):

$$\frac{\lambda}{\Delta\lambda} = \frac{N\lambda}{Q} = 2lN\lambda \ , \qquad \text{(A.13)}$$

where it is assumed that the light path is normal to the reflecting surfaces. For a given wavelength the finesse N of the instrument is usually a fixed quantity so that the spacing l is the only free parameter which can be adjusted to obtain the appropriate resolution.

The choice of the spacing is also determined in part by the calibration requirements. To be suitable for use as a calibration line, a line must be intense, and well isolated from other lines of the same gas. It must also be distant from the measured line, at the spacing chosen, by a number of orders approximately equal to a small integer and a half; this way the measured line will appear at the center of the scan when the calibration line is set to appear at both ends. Since there are not very many lines, in the rare gas lamps used for calibration, that satisfy even the first two requirements, the third one is often satisfied by changing the order number by a small amount.

Finally, because the circular variable filter has a relatively large bandpass, it may be desirable to avoid extraneous lines, emitted by the atmosphere or by the source itself, by choosing a spacing such that these lines will be well separated from the line of interest. In particular, for most of the observations presented in this thesis, the chopping has been done against the back of the

chopper wheel acting as a blackbody; it did not, therefore, provide sky subtraction. It has been necessary, then, to measure the atmospheric emission independently and to subtract its contribution from the spectra of H_2. This subtraction is quite accurate because the strongest atmospheric lines appeared at both ends of the scans and could be removed by visual comparison of the spectra.

The wavelengths of the $v=1\rightarrow 0$ $S(0)$ and $v=2\rightarrow 1$ $S(1)$ lines are at a short distance from each other with respect to the bandwith of the circular variable filter. In this case also, it has been necessary to choose a spacing for which their profiles were well separated.

Finally, the lines of HeI at 2.112 μm could contaminate the spectrum of the $v=1\rightarrow 0$ $S(1)$ line of H_2. In Orion, however, it has been determined both from the measurements of Peimbert & Costero (1969) and recombination theory (Brocklehurst 1972), and from the observed spectra of the $v=1\rightarrow 0$ $S(1)$ line, that the contribution of the He lines is negligible.

e) Measurement of the Spacing and Non-Linearity.

The value of the spacing is obtained by calibrating against each other many lines of the rare gases Ne, Ar, Kr and Xe which have accurate wavelengths. The preferred procedure in this case is to alternate measurements of the line used for calibration with the measurements of the other lines. If these measurements are made in rapid succession, any drift is canceled to very high accuracy.

The following quantities are defined:

Scan position	x_1	x_2	x_3
Wavelength	λ_1	λ_2	λ_1
Spacing (actual) =	$(n_1 + 1)\lambda_1$	$n_2\lambda_2$	$n_1\lambda_1$

$$\textit{Spacing (assumed)} = \qquad 2l + \lambda_1 \qquad 2l + \lambda_1 f\left(\frac{x_3 - x_2}{x_3 - x_1}\right) \qquad 2l$$

where x_1, x_2, x_3 are increasing values of the scan position, corresponding to decreasing values of the spacing. If the scan is linear, then

$$f\left(\frac{x_3 - x_2}{x_3 - x_1}\right) = \frac{x_3 - x_2}{x_3 - x_1} \quad . \tag{A.14}$$

The quantities n_1 and n_2 are the order numbers corresponding to λ_1 and λ_2 respectively and their difference n, defined as

$$n \equiv n_1 - n_2 \quad , \tag{A.15}$$

is evaluated according the following rule:

$$n \textit{ is the largest integer smaller or equal to } X_n \equiv 2l\left(\frac{1}{\lambda_1} - \frac{1}{\lambda_2}\right) \quad . \tag{A.16}$$

so that

$$\lambda_2 > \lambda_1 \rightarrow n \geq 0 \quad ; \quad \lambda_2 < \lambda_1 \rightarrow n < 0 \quad . \tag{A.17}$$

There may be some ambiguity, however, as to the value of n if X_n is very close to an integer. In such a case the following rules are used:

$$x_2 \approx x_1 \quad \rightarrow \quad n \approx X_n - 1 \quad , \tag{A.18}$$

$$x_2 \approx x_3 \quad \rightarrow \quad n \approx X_n \quad . \tag{A.19}$$

It is straightforward to derive from the above relations the value of the order number of λ_1 at the end of the scan, once the scan has been linearized:

$$n_1 = \frac{n\lambda_2 + \lambda_1\left(\frac{x_3 - x_2}{x_3 - x_1}\right)}{\lambda_2 - \lambda_1} \quad . \tag{A.20}$$

The advantage of this procedure is that the spacing l needs to be known only approximately (*e.g.* 1%) in order to find the right value of n, according to rule (A.16), since n is usually much smaller than n_1 and n_2. If l is not known to that

accuracy, it is possible to calculate n_1 for a pair of lines close in wavelength, in which case n is small, then obtain a more accurate value of l from n_1, and finally calculate the values of n for pairs of lines more distant in wavelength.

In order for equation (A.20) to be valid, the scans must have been linearized. The non-linearity correction itself can be evaluated from the spacing measurements, once a consistent value of the order numbers of the various lines has been found. The knowledge of the wavelength and of the order number of a line gives the actual spacing between the plates at that position along the scan where the line is detected. The comparison of scan positions with actual spacings is a direct measure of the non-linearity. The correction function was obtained as a third order polynomial:

$$x' = A_0 + A_1 x + A_2 x^2 + A_3 x^3 \quad , \tag{A.21}$$

with the coefficients

$$A_0 = 2.0145 \times 10^{1} \quad , \tag{A.21a}$$

$$A_1 = 8.1195 \times 10^{-1} \quad , \tag{A.21b}$$

$$A_2 = 2.6688 \times 10^{-4} \quad , \tag{A.21c}$$

$$A_3 = -9.5349 \times 10^{-8} \quad . \tag{A.21d}$$

The scale of x used with these coefficients is such that the full amplitude of the scan has a length of 1022., corresponding to the number of channels in the memory of the multichannel analyzer. In addition, this function is set so that

$$x = 130. \rightarrow x' = 130. \quad ; \quad x = 940. \rightarrow x' = 940. \quad . \tag{A.21e}$$

This last convention is for ease of calibration, since the amplitude and starting point of the scans are usually set so that the calibration lines are centered near these values. The non-linearity has been measured for a scanning amplitude of

1.25 spectral ranges and a scanning time of 20.5 seconds. Since the non-linearity probably depends to some extent on the amplitude and period of the scan, all the measurements presented in this thesis have been made with values close to the above. It has been shown, however, that reducing the scanning time to 10 seconds does not affect the non-linearity appreciably.

The two tables below show a sample of actual spacing measurements, made on 4 February 1980. The first table gives a list of the spectral lamps and CVF settings found useful for the spacing measurements, and shows the sequence in which they are measured and the wavelengths and approximate amplitude of the lines appearing in each scan. In this example, the line of Kr at $\lambda 2.1165471\,\mu m$ is used for the calibration of the H_2 measurements, and has been set near channels 130 and 940. The second table shows a sample of the spacing calculations made from these measurements. The symbols used in the headings of Table A.3 correspond to the quantities defined at the beginning of this section. The quantities x_1, x_2, x_3 and n_1 have been from the unlinearized scans, while x_1', x_2', x_3' and n_1' follow from the calibration and linearization procedures. The measurements in Table A.3 have been selected to illustrate the following characteristics:

1) A comparison of the values of X_n and n shows the application of rules A.16 and A.18.

2) The values of n_1 show the inconsistencies encountered when using unlinearized data. The agreement among the values of n_1' is typical and so is the fact that, on average, these values tend to be bigger than the integer. This could indicate a residual non-linearity.

3) The discrepancy between the last measurement of n_1' and the other ones,

TABLE A.2. Spectral Line Measurements.

Spectral Lamp	CVF Setting	Gain db	Scans	Wavelength μm	Relative Intensity
Krypton	627	20	2	2.1165471	
Krypton	578	20	3	2.0423964	54
				2.0446971	52
Krypton	627	20	2		
Krypton	667	10	2	2.1902513	
Krypton	627	20	2		
Krypton	699	30	6	2.2485775	83
				2.1902513	52
Krypton	627	20	2		
Argon	635	30	4	2.1332885	162
				2.0986111	62
				2.1534207	65
Krypton	627	20	3		
Argon	615	10	2	2.0986111	
Krypton	627	20	2		
Argon	646	30	2	2.1534207	
Krypton	627	20	2		
Argon	669	30	4	2.2077181	123
				2.2039561	65
Krypton	627	20	2		
Argon	677	30	4	2.2077181	600
				2.2039561	173
Krypton	627	20	3		
Argon	594	20	2	2.0616229	
Krypton	627	20	2		
Neon	656	20	4	2.1708145	
Krypton	627	20	2		
Neon	618	20	2	2.1041295	
Krypton	627	20	2		
Neon	579	20	4	2.0350238	
Krypton	627	20	2		
Xenon	574	20	2	2.0262242	
Krypton	627	20	2		
Xenon	642	20	4	2.1470089	
Krypton	627	20	2		

however, is probably due to a difference between the phase shifts of λ_1 and λ_2 at the reflecting surfaces. This difference is probably related to the lower reflectance of the plates at wavelengths below $\sim 2.08\,\mu m$. On the other

TABLE A.3. Spacing Calculations.

λ_1 λ_2 λ_1	X_n	n	x_1 x_2 x_3	n_1	x_1' x_2' x_3'	n_1'
2.1165471 2.1902513 2.1165471	37.45	37	144.84 615.65 954.72	1111.5	130.0 583.70 940.0	1112.2
2.1165471 2.0986111 2.1165471	-9.51	-10	142.73 574.43 952.86	1114.9	130.0 543.45 940.0	1112.3
2.1165471 2.2077181 2.1165471	45.96	45	143.43 169.25 953.42	1112.2	130.0 152.78 940.0	1112.2
2.1165471 2.0262242 2.1165471	-49.61	-50	140.02 666.22 951.26	1113.4	130.0 640.09 940.0	1112.98

hand, measurements that were not sensitive to the non-linearity of the scan, have failed to show any evidence of difference in the phase shifts for wavelengths between 2.11 and 2.17 μm. This effect is therefore neglected in the data analysis.

4) The uncertainty in the non-linearity correction is estimated to be equivalent to $\sim 1\,\mathrm{km\ s^{-1}}$, near the center of the scan. The correction function could probably be improved by using more measurements at different spacings.

f) Procedure for Astronomical Observations.

1) The alignment of the Fabry-Pérot is checked with a laser beam, and any necessary mechanical alignment is performed. The Fabry-Pérot is then installed in the instrument, plugged into the ramp generator and aligned piezoelectrically. The voltage ramp is turned on and left running continuously until the instrument is taken off the telescope or the spacing of the Fabry-Pérot is changed. This first step of the procedure is given a priority

more or less equal to that of cooling the detector, so that the Fabry-Pérot has time to come to thermal equilibrium and to stabilize. Its alignment is checked occasionally during this period.

2) The dewar is aligned with respect to the rest of the instrument by centering the focal plane diaphragm in the dewar with that behind the chopper wheel ((a) and (g) in Figure 1).

3) After the detector and the data recording apparatus have been installed, the amplitude of the scan and its starting point are set to their proper values. As time permits, some measurements of the spacing are done before starting the observations, in case the decision is made to change the spacing during the night, when a minimum loss of time is desirable.

4) The next step is to point to a bright star and to find the position of the signal and reference beams on the sky, with respect to the pointing of the telescope. While guiding on this star, the dewar is tipped to maximize the signal. The usual adjustment of the phase of the lock-in amplifier is also done.

5) After the telescope has been moved to the source, the alignment of the Fabry-Pérot must be adjusted, to correct for the change of its orientation with respect to the direction of the force of gravity. When checking the alignment, it is useful to have the diaphragm (g) closed to the size of a pinhole. It is important, however, to leave it fully open for all other measurements. It is also very important not to forget to move the beam splitter (f) away from the beam after realigning. Omitting to reopen the diaphragm or to turn away the beamsplitter will result in a much weaker signal being detected from the calibration lamp, providing a form of fail-safe. This is not the case, however, for the mirror (k) used to inject into the beam the light from the calibration lamp, and the observer must be careful not to

forget to remove this mirror before observing an astronomical object.

6) During the observations, the stability of the Fabry-Pérot normally is such that realignment is needed every 1-2 hours. Excessive drifts of the calibration lines is an indication of the need for realignment. Drifts of 2, 5, 8 channels are respectively good, average and poor for a 15 minute interval, when one free spectral range extends over 810 channels. The decision to reduce the effect of the drifts by increasing the frequency of the calibration measurements depends on whether the precision of the measurements is limited by the calibration or by the signal-to-noise. In the latter case it is better to limit the time spent for calibration. After correction of the alignment, the starting point of the scan is reset to the chosen value.

7) A typical sequence of measurements is shown in the example of the logbook format, Table A.4. Below each title is a number giving the suggested width of the column. The use of each column is outlined below:

Comments: seeing, guide star identification, estimates of misalignments, etc..

ALIGN: indicates when the alignment has been checked.

X,Y: give the offset guider coordinates, or the positions of the lines in the calibration and spacing measurement scans. These approximate positions are useful as input for the calibration program.

Last Record: indicates the number of the last record of the current file on the magnetic tape corresponding to this measurement. For safety, each measurement is recorded twice on the tape. In case of doubt, of course, more records are better than less. These record numbers are useful when relating the output

from the magnetic tape to the logbook data; they start from the beginning of the current file only. Errors in these numbers are not of much consequence but each end-of-file mark put on the tape must be recorded in this column. An end-of-file mark is put on the tape at least at the end of each night and ideally a few times during the night. Before the tape is removed from the tape recorder, ~ 6 end-of-file marks are recorded.

H2Data: this column is left blank during the observing run; it is used for the number of the corresponding record on the master tape. The name of the master tape should replace the name "H2Data" in the title of this column.

OBJECT: self explanatory.

AP: diaphragm.

CVF: circular variable filter setting.

G: gain.

τ: time constant of the lock-in amplifier. It is set to a low enough value to avoid causing an asymmetry of the line profiles.

VFS: is the volt-full-scale setting of the analog-to-digital converter of the multichannel analyzer.

T Scan: period of one scan.

No. Scans: number of scans co-added in the measurement.

PST: Pacific Standard Time.

V Helio.: velocity correction for transformation from the observed velocity to heliocentric (or LSR) velocity. This column is usually filled at a later time; the value of the correction is obtained from PST and the coordinates of the object.

8) Care must be taken to make sure that the data are transferred properly to the tape recorder. Problems have arisen due to improper contacts between the connector and the plug on the multichannel analyzer. A good check is to fill the memory of the analyzer with one of the following values: 1, 2, 4, 8, 16, 32, and to check that the corresponding channel indicator light on the recorder is turned on at the end of the data transfer. (This paragraph applies to the Cipher tape recorder used with the Nicolet multichannel analyzer).

g) Data Reduction.

The data reduction is done in three steps:

1) The first program reads the magnetic tapes recorded at the observatory, compares the records, gets rid of exact duplicates, transfers all the remaining records to two master tapes and prints them out.

2) After the correspondence between the master tape record numbers and the logbook data have been noted, the second program finds the position of the lines in the calibration scans and in the spacing measurement scans.

3) The third program calibrates the data scans, corrects for the non-linearity, corrects for the variations of the heliocentric correction, adds together all measurements of the same object and plots and records the resulting spectra.

For convenience in filing the printed output from these programs, the first program is named "FABmmmya", the second one "CALmmmya", and the third one "DATmmmya", where "mmm" stands for the abbreviation of the month of the observations, "y" stands for the last digit of the year, and "a" is a letter which is useful to distinguish between different reruns of the program during the same

month (for the same or different data).

REFERENCES

Brocklehurst, M. 1972, *M. N. R. A. S.*, **157**, 211.

Jacquinot, P. 1960, *Rept. Prog. Phys.*, **23**, 267.

Outred, M. 1978, *J. Phys. Chem. Ref. Data*, **7**, 1.

Peimbert, M. and Costero, R. 1969, *Bol. Obs. Tonantzintla y Tacubaya*, **5**, 3.

Vaughan, A.H. 1967, *Ann. Rev. Astron. Astrophys.*, **5**, 139.

TABLE A.4. Logbook Format.

19 NOV 1980 PALOMAR (20)	ALIGN (1)	X (5)	Y (5)	Last Record (3)	H2Data File 2 (4)	OBJECT (12)	AP (2)	CVF (3)	G (2)	τ (3)	VFS (3)	T Scan (2)	NO. Scans (3)	PST (4)	V Helio. (4)
		54.5	134.5	22	63	T TAU +	40	627	60	.015	± 8	10	32	0105	4.03
				24	64	T TAU −	|	|	60	|	|	|	32	0113	
		61	477	26	65	KR	|	|	20	|	|	|	2		
no change needed---→	✓						↓	↓		↓	↓	↓			
		58	475	28	66	KR			20				2		
				30	67	T TAU +			60				32	0126	
				32	68	T TAU −			60				32	0133	
		59	475	34	69	KR			20				2		
				36	70	T TAU +			60				32	0142	
				38	71	T TAU −			60				32	0149	
		61	477	40	72	KR			20				2		
				42	73	T TAU +			60				32		
				44	74	T TAU −			60				32	0203	
		64	480	46	75	KR			20				2		
Center on HH1* Offset S98.5,E74 to HH2E				EOF8											
needed realignment---→	✓														
		62	478	3	76	KR			20				2		
				5	77	HH2E +			60				32	0246	
				7	78	HH2E −			60				32	0253	
		60	478	9	79	KR			20				2		
Sky quite clear now				11	80	HH2E +			60				32	0302	
				13	81	HH2E −			60				32	0308	
		61	479	15	82	KR			20				2		
				17	83	HH2E +			60				32	0318	
				19	84	HH2E −			60				32	0324	
		63	480	21	85	KR			20				2		
leave as is---→	✓														
		61	480	23	86	KR			20				2		
				25	87	HH2E +			60				32	0343	10.39
				27	88	HH2E −			60				32	0350	
		64	481	29	89	KR			20				2		
				31	90	HH2E +			60				32	0359	
Airmass 1.80				33	91	HH2E −			60				32	0406	
		64	482	35	92	KR			20				2		